

Extended and improved criss-cross algorithms for computing the spectral value set abscissa and radius

Peter Benner* Tim Mitchell*

September 6th, 2019

Abstract

In this paper, we extend the original criss-cross algorithms for computing the ε -pseudospectral abscissa and radius to general spectral value sets. By proposing new root-finding-based strategies for the horizontal/radial search subphases, we significantly reduce the number of expensive Hamiltonian eigenvalue decompositions incurred, which typically translates to meaningful speedups in overall computation times. Furthermore, and partly necessitated by our root-finding approach, we develop a new way of handling the singular pencils or problematic interior searches that can arise when computing the ε -spectral value set radius. Compared to would-be direct extensions of the original algorithms, that is, without our additional modifications, our improved criss-cross algorithms are not only noticeably faster but also more robust and numerically accurate, for both spectral value set and pseudospectral problems.

1 Introduction

Consider the continuous-time linear dynamical system

$$E\dot{x} = Ax + Bu, \quad (1a)$$

$$y = Cx + Du, \quad (1b)$$

where $A \in \mathbb{C}^{n \times n}$, $B \in \mathbb{C}^{n \times m}$, $C \in \mathbb{C}^{p \times n}$, $D \in \mathbb{C}^{p \times m}$, and $E \in \mathbb{C}^{n \times n}$ is assumed to be invertible. Using output feedback $u = \Delta y$, where $\Delta \in \mathbb{C}^{m \times p}$, so that input u varies linearly with respect to output y , (1a) can be rewritten as $E\dot{x} = Ax + B\Delta y$ and (1b) as $y = (I - D\Delta)^{-1}Cx$, assuming $(I - D\Delta)$ is invertible. Thus, the input-output system (1) is equivalent to

$$E\dot{x} = M(\Delta)x, \quad (2)$$

where

$$M(\Delta) := A + B\Delta(I - D\Delta)^{-1}C \quad (3)$$

is called the *perturbed system matrix*. As a consequence, the dynamical properties of (1), which arise in many engineering applications, can be studied by examining the generalized eigenvalue problem of the matrix pencil $(M(\Delta), E) = \lambda E - M(\Delta)$.

For the special case of $B = C = E = I_n$, where I_n is the $n \times n$ identity matrix, and $D = 0$, (2) simply reduces to

$$\dot{x} = (A + \Delta)x. \quad (4)$$

*Max Planck Institute for Dynamics of Complex Technical Systems, Magdeburg, 39106 Germany
benner@mpi-magdeburg.mpg.de, mitchell@mpi-magdeburg.mpg.de.

Considering $\Delta = 0$, the ordinary differential equation $\dot{x} = Ax$ is asymptotically stable if its *spectral abscissa*, the maximal real part attained by the eigenvalues of matrix A , is strictly negative: $\alpha(A) < 0$. However, the spectrum only provides a limited perspective with respect to the dynamics of the system. If matrices close to an asymptotically stable matrix A have eigenvalues in the right half plane, then the solution of $\dot{x} = Ax$ may still have large transient behavior before converging. Furthermore, in applications, where A models some physical process or mechanism, the theoretical asymptotic stability of A may not be predictive of reality, particularly if small perturbations of the model A can result in unstable systems. Hence, there has been great interest to also consider the dynamical properties of (4), which is characterized by *pseudospectra* [TE05]: the set of eigenvalues of A under general perturbation, typically limited by placing an upper bound on the spectral norm of Δ . For a given $\varepsilon \geq 0$, the ε -*pseudospectral abscissa*:

$$\alpha_\varepsilon(A) := \max\{\operatorname{Re} \lambda : \lambda \in \sigma(A + \Delta), \|\Delta\|_2 \leq \varepsilon\},$$

where $\sigma(\cdot)$ denotes the spectrum, provides a measure of *robust stability*: if $\alpha_\varepsilon(A) < 0$, then $A + \Delta$ is stable for any perturbation such that $\|\Delta\|_2 \leq \varepsilon$. The norm of the smallest destabilizing perturbation, i.e., the value of ε that yields $\alpha_\varepsilon(A) = 0$, is called the *distance to instability*, introduced by [Van85]. Beyond robust stability measures, pseudospectra also provide information about the transient behaviors of dynamical systems [TE05, Chs. 14-19]. For example, [TTRD93] proposed pseudospectra as a tool for analyzing how laminar flows transition to turbulence, by looking not just at spectra but pseudospectra of (stable) linearizations of the nonlinear problem.

Computationally, numerous techniques for plotting the boundaries of pseudospectra are discussed in [Tre99, WT01], while a “criss-cross” algorithm for computing the ε -pseudospectral abscissa to high precision, with a local quadratic rate of convergence, was proposed in [BLO03]. The criss-cross algorithm performs a sequence of alternating vertical and horizontal searches to find relevant boundary points of the ε -pseudospectrum along the respective search lines, which converge to a globally rightmost point of the ε -pseudospectrum; these vertical and horizontal searches are accomplished by computing eigenvalues of associated Hamiltonian matrices or matrix pencils. In fact, the techniques used in the criss-cross algorithm build upon those developed for the first algorithm for computing the distance to instability [Bye88]. Relevant for discrete-time systems $x_{k+1} = Ax_k$, the criss-cross algorithm has also been adapted to compute the corresponding ε -*pseudospectral radius*:

$$\rho_\varepsilon(A) := \max\{|\lambda| : \lambda \in \sigma(A + \Delta), \|\Delta\|_2 \leq \varepsilon\},$$

by using circular and radial searches instead of vertical and horizontal ones [MO05]. Of course, when $\varepsilon = 0$, $\rho_\varepsilon(A) = \rho(A)$, the *spectral radius* of A .

For the more general setting of (1), the analogue of the ε -pseudospectrum is an ε -*spectral value set* while the analogue of the distance to instability is the *complex stability radius* (perhaps better known by its reciprocal value, the \mathcal{H}_∞ norm). Spectral value sets are distinctly different from pseudospectra of generalized eigenvalue problems $\lambda E - A$, where both A and E could be considered under general perturbation. In spectral value sets, (1) only permits *structured* perturbations of the form $B\Delta(I - D\Delta)^{-1}C$ to operator A , while E remains unperturbed. Fixed matrices A , B , C , D , and E represent the certainties of the model while Δ represents the uncertainties in the feedback loop. To identify dynamical properties of (1), it is natural to consider the worst outcome possible over the set of uncertainties. The complex stability radius encodes precisely that: the norm of the smallest matrix Δ such that $B\Delta(I - D\Delta)^{-1}C$ destabilizes (1), assuming for now that (A, E) is stable itself.

Algorithms for computing the complex stability radius (or the \mathcal{H}_∞ norm) of general systems with input and output (1) also generally rely on extensions of the level set techniques developed by [Bye88] for computing the distance to instability. Like the pseudospectral abscissa and radius algorithms, these too require $\mathcal{O}(n^3)$ amount of work and $\mathcal{O}(n^2)$ memory per iteration so there has been much recent interest in developing alternative scalable approximation techniques. Spectral

value sets have been a useful tool in this endeavor (see [GGO13, BV14, MO16]), even though exact methods have not made use of them (at least not directly). The key component has been the introduction of efficient iterations for approximating the ε -spectral value set abscissa, which was first done for approximating the ε -pseudospectral abscissa (and radius) in [GO11].

In this work, we extend the pseudospectral methods of [BLO03, MO05] to computing the spectral value set and radius, thus providing dense and exact analogues to the above scalable approximation techniques. We also propose significant modifications and improvements to these methods. The core idea is one we simultaneously exploited in our work to accelerate the computation of the \mathcal{H}_∞ norm [BM18]: replace large Hamiltonian eigenvalue computations with much cheaper evaluations of the norm of the transfer function wherever possible. However, while [BM18] uses a rather straightforward application of smooth optimization techniques to take larger (and thus fewer) steps before converging to the \mathcal{H}_∞ norm, our work here involves several important differences and additional complexities. First, we replace the globally-optimal horizontal/radial searches in the original algorithms with much cheaper but possibly only locally-optimal root-finding-based searches (using the norm of the transfer function); consequently, our new algorithms could conceivably incur more iterations than the original methods, even though they are often significantly faster overall. Second, our new approach also affords a new strategy to intelligently order the horizontal/radial searches so that relatively few are actually solved per iteration and those that are solved are all warm started by increasingly better initializations. Third, as the original pseudospectral radius algorithm requires globally-optimal radial searches to ensure it does not stagnate, we additionally propose a new technique for overcoming the problematic singular pencils and interior searches that may arise, one that is both compatible with our new locally-optimal radial searches and that should also be more robust in practice. While our modifications only affect the constant factors in terms of efficiency, the resulting speedups are nevertheless typically meaningful. For example, in robust control applications, the spectral value set (or pseudospectral) abscissa/radius can appear as part of a nonsmooth optimization design task and will thus be typically evaluated thousands or even millions of times during optimization. Finally, by no longer computing purely imaginary eigenvalues of Hamiltonian eigenvalue problems for the horizontal/radial searches, our new methods also avoid the accompanying rounding errors of such computations; as a result, our improved methods are more reliable and accurate in practice.

The paper is organized as follows. Prerequisite definitions and theory are given in §2. In §3, we directly extend the pseudospectral abscissa algorithm of [BLO03] to the spectral value set abscissa and then present our corresponding improved method in §4. We respectively do the same for the pseudospectral radius algorithm of [MO05] and the spectral value set radius in §5 and §6, the latter of which includes our new way of handling singular pencils and interior searches. Convergence results are given in §7, while implementation details and numerical experiments are respectively provided in §8 and §9. Concluding remarks are made in §10.

2 Spectral value sets and the transfer function

The following general concepts are used throughout the paper.

Definition 2.1. *Given a nonempty closed set $\mathcal{D} \subset \mathbb{C}$, a point $\lambda \in \mathcal{D}$ is:*

1. rightmost if $\operatorname{Re} \lambda = \max\{\operatorname{Re} z : z \in \mathcal{D}\}$
2. outermost if $|\lambda| = \max\{|z| : z \in \mathcal{D}\}$
3. isolated if $\mathcal{D} \cap \mathcal{N} = \lambda$ for some neighborhood \mathcal{N} of λ
4. interior or strictly inside if $\mathcal{N} \subset \mathcal{D}$ for some neighborhood \mathcal{N} of λ .

Furthermore, λ is a locally rightmost or outermost point of \mathcal{D} if λ is respectively a rightmost or outermost point of $\mathcal{D} \cap \mathcal{N}$, for some neighborhood \mathcal{N} of λ .

Definition 2.2. Let $\varepsilon \geq 0$ be such that $\varepsilon\|D\|_2 < 1$ and define the ε -spectral value set

$$\sigma_\varepsilon(A, B, C, D, E) = \bigcup \{\sigma(M(\Delta), E) : \Delta \in \mathbb{C}^{m \times p}, \|\Delta\|_2 \leq \varepsilon\}. \quad (5)$$

Remark 2.3. Note that we assume that E is invertible, here and throughout the paper. If E is singular but (A, E) is still index 1, then the system can be transformed into an equivalent representation without a singular E matrix; see [FRM08] for details.

Now consider the transfer function associated with input-output system (1):

$$G(\lambda) := C(\lambda E - A)^{-1} + D \quad \text{for } \lambda \in \mathbb{C} \setminus \sigma(A, E). \quad (6)$$

As shown in [HP05, §5.2] for $E = I$, spectral value sets can be equivalently defined in terms of the norm of the transfer function, instead of eigenvalues of $(M(\Delta), E)$. This fundamental result easily extends to the case of generic E matrices we consider here; e.g. the proof of [GGO13, Theorem 2.1] readily generalizes by substituting all occurrences of $(\lambda I - A)$ with $(\lambda E - A)$.

Theorem 2.4. Let $\varepsilon \geq 0$ be such that $\varepsilon\|D\|_2 < 1$ and $\|\Delta\|_2 \leq \varepsilon$ so that $I - D\Delta$ is invertible. Then for $\lambda \notin \sigma(A, E)$ the following are equivalent:

$$\|G(\lambda)\|_2 \geq \varepsilon^{-1} \quad \text{and} \quad \lambda \in \sigma(M(\Delta), E) \text{ for some } \Delta \text{ with } \|\Delta\|_2 \leq \varepsilon. \quad (7)$$

By Theorem 2.4, the following corollary is immediate, providing an alternate spectral value set definition based on the norm of the transfer function.

Corollary 2.5. Let $\varepsilon \geq 0$ be such that $\varepsilon\|D\|_2 < 1$. Then

$$\sigma_\varepsilon(A, B, C, D, E) = \sigma(A, E) \bigcup \{\lambda \in \mathbb{C} \setminus \sigma(A, E) : \|G(\lambda)\|_2 \geq \varepsilon^{-1}\}. \quad (8)$$

Note that the nonstrict inequalities in Definition 2.2 and Theorem 2.4 imply that the spectral value sets we consider are compact. Furthermore, the boundary of $\sigma_\varepsilon(A, B, C, D, E)$ is characterized by the condition $\|G(\lambda)\|_2 = \varepsilon^{-1}$ while for any matrix Δ such that $\lambda \in \sigma(M(\Delta), E)$ is a boundary point, $\|\Delta\|_2 = \varepsilon$ must hold (though the reverse implication is not true).

Lemma 2.6. Let $\varepsilon > 0$ be such that $\varepsilon\|D\|_2 < 1$ and let λ be a non-isolated boundary point of an ε -spectral value set, with associated perturbation matrix Δ , that is, $\lambda \in \sigma(M(\Delta), E)$. Then for one or more $\lambda_0 \in \sigma(A, E)$, there exists a continuous path parameterized by $t \in [0, 1]$ such that $\lambda(t)$ is an eigenvalue of $\sigma(M(t\Delta), E)$ taking $\lambda(0) = \lambda_0$ to $\lambda(1) = \lambda$. Furthermore, $\lambda(t)$ is only a boundary point at $t = 1$.

Proof. By continuity of eigenvalues, the continuous path $\lambda(t)$ exists and clearly, $\|t\Delta\|_2 < \|\Delta\|_2$ holds for $t \in [0, 1)$. As λ is on the boundary, $\|\Delta\|_2 = \varepsilon$ holds but then the necessary condition for $\lambda(t)$ to be a boundary point is violated for all $t \in [0, 1)$. \square

2.1 The spectral value set abscissa and radius

The ε -spectral value set abscissa, relevant for continuous-time systems (1), is formally defined as follows.

Definition 2.7. Let $\varepsilon \geq 0$ be such that $\varepsilon\|D\|_2 < 1$ and define the ε -spectral value set abscissa

$$\alpha_\varepsilon(A, B, C, D, E) := \max\{\operatorname{Re} \lambda : \lambda \in \sigma_\varepsilon(A, B, C, D, E)\}. \quad (9)$$

Now consider the discrete-time linear dynamical system

$$Ex_{k+1} = Ax_k + Bu_k \quad (10a)$$

$$y_k = Cx_k + Du_k, \quad (10b)$$

where the matrices are defined as before in (1). For the case when $B = C = E = I_n$, and $D = 0$, the simple ordinary difference equation $x_{k+1} = Ax_k$ is asymptotically stable if and only if its *spectral radius*, the maximal modulus attained by the eigenvalues of A , is strictly less than one: $\rho(A) < 1$. Thus, for discrete-time input-output systems of the form of (10), we generalize the ε -pseudospectral radius as follows.

Definition 2.8. Let $\varepsilon \geq 0$ be such that $\varepsilon\|D\|_2 < 1$ and define the ε -spectral value set radius

$$\rho_\varepsilon(A, B, C, D, E) := \max\{|\lambda| : \lambda \in \sigma_\varepsilon(A, B, C, D, E)\}. \quad (11)$$

However, for input-output systems, there is an additional wrinkle when defining the ε -spectral value set abscissa and radius: eigenvalues may not be of interest if they are not *controllable* and *observable*, concepts which we now define.

Definition 2.9. Let λ be an eigenvalue of the matrix pencil (A, E) from an input-output system. Eigenvalue λ is *observable* if $Cx \neq 0$ holds for all of its right eigenvectors x , i.e. $Ax = \lambda Ex, x \neq 0$. Eigenvalue λ is *controllable* if $B^*y \neq 0$ holds for all of its left eigenvectors y , i.e. $y^*A = \lambda y^*E, y \neq 0$.

In a sense, the presence of uncontrollable and/or unobservable eigenvalues can be considered an artifact of redundancy in a specific system design. Any associated transfer function $G(\lambda)$ of (1) with uncontrollable or unobservable eigenvalues can be reduced to what is called a *minimal realization* $\widehat{G}(\lambda)$, whose eigenvalues are all controllable and observable; e.g. see [Dai89, Theorem 2-6.3]. The A and E matrices of $\widehat{G}(\lambda)$ are of minimal possible dimension so that the reduced transfer function is unaltered and its input-output behavior remains identical to $G(\lambda)$.

In terms of spectral value sets, consider an eigenvalue λ of (A, E) with right and left eigenvectors x and y . If λ is unobservable or uncontrollable, then $Cx = 0$ or $B^*y = 0$ respectively holds, and thus for any perturbation matrix $\Delta \in \mathbb{C}^{m \times p}$, either $M(\Delta)x = Ax$ or $y^*M(\Delta) = y^*A$ holds. Furthermore, if λ is a simple eigenvalue, then for sufficiently small $\varepsilon > 0$, λ must be an isolated point of $\sigma_\varepsilon(A, B, C, D, E)$: letting $\lambda(t)$ be some parameterization of λ with $t \in \mathbb{R}$ and $\lambda(0) = \lambda$, via standard perturbation theory for simple eigenvalues, it is easily seen that $\lambda'(0) = 0$ holds.

Since the presence of uncontrollable/unobservable eigenvalues will only affect the point in the complex plane used to initialize the algorithms presented here (and such eigenvalues can be removed as a preprocessing step), for the remainder of the paper we simply assume whether or not they are included is determined by the user.

2.2 Derivatives of the norm of the transfer function

As we will utilize first- and second-order information of $\|G(\lambda)\|_2$ in different ways, we will need the following results. For technical reasons, we will first need the following assumption.

Assumption 2.10. Let $\varepsilon > 0$ with $\varepsilon\|D\|_2 < 1$ and let $\lambda \in \sigma_\varepsilon(A, B, C, D, E)$ with $\lambda \notin \sigma(A, E)$. Then the largest singular value of $G(\lambda)$ is simple.

Remark 2.11. For almost all quintuplets (A, B, C, D, E) , the largest singular value of $G(\lambda)$ is indeed simple for all $\lambda \in \mathbb{C} \setminus \sigma(A, E)$; e.g. see [BLO03, §2] for pseudospectra and [GGO13, Remark 2.20] for general spectral value sets with $E = I$. Although counter examples can be constructed (see [GGO13, Remark 2.20]), with probability one such examples will not be encountered in practice and as such, this technicality does not pose a problem for the algorithms we propose here.

Let $\lambda(t) \in \mathbb{C}$ be parameterized with respect to $t \in \mathbb{R}$ and $Z(t) = \lambda(t)E - A$. Then

$$(G \circ \lambda)(t) = C(\lambda(t)E - A)^{-1}B + D = CZ(t)^{-1}B + D. \quad (12)$$

By standard (matrix) differentiation techniques, we have that:

$$(G \circ \lambda)'(t) := -\lambda'(t)CZ(t)^{-1}EZ(t)^{-1}B \quad (13a)$$

$$(G \circ \lambda)''(t) := 2\lambda'(t)^2CZ(t)^{-1}EZ(t)^{-1}EZ(t)^{-1}B - \lambda''(t)CZ(t)^{-1}EZ(t)^{-1}B. \quad (13b)$$

Furthermore, let $s(t)$ be the largest singular value of (12), i.e. $\|G(\lambda(t))\|_2$, with associated left and right singular vectors $u(t)$ and $v(t)$. Assuming that $s(t)$ is a simple singular value at say, $t = 0$, by standard perturbation theory, it follows that

$$s'(0) = \operatorname{Re}(u(0)^* [(G \circ \lambda)'(0)] v(0)) \quad (14a)$$

$$= -\operatorname{Re}(u(0)^* [\lambda'(0)CZ(0)^{-1}EZ(0)^{-1}B] v(0)). \quad (14b)$$

To compute $s''(0)$, we need the following result for the second derivative of eigenvalues, which can be found in various forms, e.g. [Lan64, OW95].

Theorem 2.12. *For $t \in \mathbb{R}$, let $H(t)$ be a twice-differentiable $n \times n$ Hermitian matrix family with distinct eigenvalues at $t = 0$ with (λ_k, x_k) denoting the k th such eigenpair and where each eigenvector x_k has unit norm and the eigenvalues are ordered $\lambda_1 \geq \dots \geq \lambda_n$.¹ Then:*

$$\lambda_1''(t) \Big|_{t=0} = x_1^* H''(0) x_1 + 2 \sum_{k=2}^n \frac{|x_1^* H'(0) x_k|^2}{\lambda_1 - \lambda_k}.$$

Since $s(t)$ is the largest singular value of $G(\lambda(t))$, it is also the largest eigenvalue of the matrix:

$$H(t) = \begin{bmatrix} 0 & G(\lambda(t)) \\ G(\lambda(t))^* & 0 \end{bmatrix}, \quad (15)$$

which has first and second derivatives

$$H'(t) = \begin{bmatrix} 0 & (G \circ \lambda)'(t) \\ ((G \circ \lambda)'(t))^* & 0 \end{bmatrix} \quad \text{and} \quad H''(t) = \begin{bmatrix} 0 & (G \circ \lambda)''(t) \\ ((G \circ \lambda)''(t))^* & 0 \end{bmatrix}, \quad (16)$$

and where the nonzero blocks are given by (13). Thus, by constructing matrix (15) and its first and second derivatives given in (16), $s''(0)$ can be computed by a straightforward application of Theorem 2.12.

Note that $s'(0)$ and $s''(0)$ are relatively cheap to compute once $s(0)$ has been. An LU factorization needed to apply $Z(0)^{-1}$ for computing $s(0)$ can be saved and reused to cheaply compute the two matrices given in (13), noting that ignoring $\lambda'(t)$, (13a) appears in (13b). Moreover, the eigenvectors x_k of (15) can be obtained from the full SVD of $G(\lambda(0))$. Let σ_k be the k th singular value of $G(\lambda(0))$ with associated right and left singular vectors u_k and v_k , respectively. Then $\pm\sigma_k$ is an eigenvalue of (15) with eigenvector $\begin{bmatrix} u_k \\ v_k \end{bmatrix}$ for σ_k and eigenvector $\begin{bmatrix} u_k \\ -v_k \end{bmatrix}$ for $-\sigma_k$. The eigenvector for $\sigma_k = 0$ is either $\begin{bmatrix} u_k \\ \mathbf{0} \end{bmatrix}$ (when $p > m$) or $\begin{bmatrix} \mathbf{0} \\ v_k \end{bmatrix}$ (when $p < m$), where $\mathbf{0}$ denotes a column of m or p zeros, respectively.

When $B = C = I_n$ and $D = 0$, the LU and backsolves can be completely avoided by instead equivalently computing the reciprocal of the smallest singular value of $\lambda E - A$. Otherwise, if $G(\lambda)$ will be evaluated at more than just a handful of points, making LU factorizations of $\lambda E - A$ for each $\lambda \in \mathbb{C}$ can also be inefficient. As shown in [Lau81] for $E = I$, one can first make an upper Hessenberg factorization of $A = PHP^*$, which is $\mathcal{O}(n^3)$ work but only needs to be done once. Then $G(\lambda)$ can be evaluated as $\tilde{C}(\lambda I - H)^{-1}\tilde{B} + D$, where $\tilde{C} = CP$ and $\tilde{B} = P^*B$; applying $(\lambda I - H)^{-1}$ only requires $\mathcal{O}(n^2)$ work as it remains Hessenberg for any $\lambda \in \mathbb{C}$. This Hessenberg technique also extends to when $E \neq I$ [VDV85].

¹ In [BM18, Remark 4.2], we were overly cautious in assuming that all the singular values of $G(\lambda(t))$ at $t = 0$ are simple; only simplicity of the largest singular value is needed.

3 Directly extending the pseudospectral abscissa algorithm

The criss-cross method of [BLO03] alternates between vertical and horizontal search phases, which we now describe and generalize to computing the spectral value set abscissa.

3.1 Vertical search

The following fundamental theorem relates singular values of the transfer function, evaluated at some point $\lambda \in \mathbb{C}$, to purely imaginary eigenvalues of an associated matrix pencil. A key tool for various stability measure algorithms, including the criss-cross method of [BLO03], this correspondence was first shown by [Bye88] for $B = C = E = I$, $D = 0$, and $x = 0$ and has previously appeared in various less general specific extensions than what we present here. We defer its proof, and that of the upcoming Theorem 3.4, to Appendix A.

Theorem 3.1. *Let $x \in \mathbb{R}$, $y \in \mathbb{R}$, $\gamma > 0$ not a singular value of D , and $\lambda E - A$ be regular. Consider the matrix pencil $(\mathcal{M}_{\gamma x}, \mathcal{N})$, where*

$$\mathcal{M}_{\gamma x} := \begin{bmatrix} A - xE - BR^{-1}D^*C & -\gamma BR^{-1}B^* \\ \gamma C^*S^{-1}C & -(A - xE - BR^{-1}D^*C)^* \end{bmatrix}, \quad \mathcal{N} := \begin{bmatrix} E & 0 \\ 0 & E^* \end{bmatrix}, \quad (17)$$

*$R = D^*D - \gamma^2 I$, and $S = DD^* - \gamma^2 I$. Then $\mathbf{i}y$ is an eigenvalue of $(\mathcal{M}_{\gamma x}, \mathcal{N})$ if and only if γ is a singular value of $G(x + \mathbf{i}y)$ and $x + \mathbf{i}y$ is not an eigenvalue of (A, E) .*

By setting $\gamma = \varepsilon^{-1}$, Theorem 3.1 immediately leads to the ability to compute all the boundary points, if any, of an ε -spectral value set that lie on any desired vertical line specified by the value of x . Given these boundary points, the subset of adjacent pairs on this vertical line which correspond to segments in the ε -spectral value set can be determined in multiple ways. While there are a few ways to do this, just evaluating the norm of the transfer function at their midpoints is a simple and robust choice.

Remark 3.2. *Note that the matrix pencil given by (17) cannot be singular. If it were, then γ would be a singular value of $G(x + \mathbf{i}y)$ for all $y \in \mathbb{R}$ and thus the entire vertical line specified by value x would be a part of $\sigma_\varepsilon(A, B, C, D, E)$. Since (A, E) is regular and ε is finite, this is not possible.*

3.2 Horizontal search

Given vertical line $x = \eta$, let $\Omega_k = [y_k, y_{k+1}]$ denote a cross section segment of $\sigma_\varepsilon(A, B, C, D, E)$ on this line and $\Omega = \{\Omega_1, \dots, \Omega_q\}$ denote the set of all such cross sections for $x = \eta$, with at least one having nonzero length. Without loss of generality, assume that interval Ω_k has nonzero length. Since any point $\eta + \mathbf{i}y$ with $y \in (y_k, y_{k+1})$ is strictly in the interior of $\sigma_\varepsilon(A, B, C, D, E)$, rightward progress within the spectral value set is indeed possible from vertical line $x = \eta$.

In [BLO03], it was proposed to consider rightward progress from the midpoints of all the positive-length vertical cross sections $\Omega_k \in \Omega$, i.e., along horizontal lines given by $\psi_k = 0.5(y_k + y_{k+1})$. The maximal rightward progress is then given by solving:

$$\max_{\Omega_k \in \Omega} \max\{\operatorname{Re} \lambda : \lambda \in \sigma_\varepsilon(A, B, C, D, E) \text{ and } \operatorname{Im} \lambda = \psi_k\}. \quad (18)$$

To solve (18), [BLO03] applied a “rotated” version of Theorem 3.1 to compute all boundary points along each horizontal line. We now present this result not only extended to spectral value sets but also to any line in the complex plane, as this more general form will be used in §5 for computing the spectral value set radius.

Definition 3.3. Let $\theta \in [0, 2\pi)$ denote the angle between the x -axis and some ray from the origin, with the positive x and y directions respectively given by $\theta = 0$ and $\theta = \pi/2$. Given $s \in \mathbb{R}$, we define $L(\theta, s)$ as the parallel line to the left of the ray given by θ , separated by distance s , with left defined with respect to the direction θ .

Theorem 3.4. Given the line $L(\theta, s)$, let $\{\mathbf{i}\omega_1, \dots, \mathbf{i}\omega_l\}$ be the set of purely imaginary eigenvalues of (17), where $\gamma = \varepsilon^{-1}$, $x = -s$, and matrices A and B have been respectively replaced by $e^{\mathbf{i}\theta_\tau} A$ and $e^{\mathbf{i}\theta_\tau} B$, with $\theta_\tau = \pi/2 - \theta$. Then the points $\lambda_j = e^{-\mathbf{i}\theta_\tau}(-s + \mathbf{i}\omega_j)$ define the cross sections of $\sigma_\varepsilon(A, B, C, D, E)$ along $L(\theta, s)$.

By Theorem 3.4, the boundary points of $\sigma_\varepsilon(A, B, C, D, E)$ along the horizontal line $L(0, \psi_k)$ are given by $\omega_j + \mathbf{i}\psi_k$, where $\{\mathbf{i}\omega_1, \dots, \mathbf{i}\omega_l\}$ are the imaginary eigenvalues (sorted in increasing order) of the rotated version of (17) given by Theorem 3.4. Thus, $\psi_k + \mathbf{i}\omega_l$ is the rightmost boundary point along line $L(0, \psi_k)$, with $\omega_l > \eta$ (assuming the corresponding cross section had positive length). Applying this procedure to each of the horizontal lines given by the ψ_k midpoints yields the solution to (18).

3.3 The complete directly-extended abscissa algorithm

Computing the pseudospectral abscissa, as originally specified in [BLO03], begins with a vertical search and then alternates between horizontal and vertical searches, to respectively increase estimate $x = \eta$ (monotonically) and find the new vertical cross sections; see Figure 1a for a visualization of this process. The procedure converges to a globally rightmost point $\lambda_* \in \sigma_\varepsilon(A)$, with $\eta_* = \text{Re } \lambda_* = \alpha_\varepsilon(A)$. A critical requirement for global convergence is that the initial vertical search must be done to the right of a globally rightmost eigenvalue of matrix A ; it cannot be done exactly through an eigenvalue of A as this would violate the conditions of Theorem 3.1 so in practice a small perturbation is used. Under a regularity assumption, the authors showed that the criss-cross method has local quadratic convergence [BLO03, §5]. The algorithm requires $\mathcal{O}(n^3)$ work and $\mathcal{O}(n^2)$ memory per iteration, both with notably large constants since it must compute all the imaginary eigenvalues of $q+1$ different matrix pencils of size $2n \times 2n$ per iteration: one pencil for the vertical search and q pencils for the corresponding q cross-sections of positive length in the horizontal search phase. Provided that a structure-preserving and backward-stable Hamiltonian eigenvalue solver is used for both vertical and horizontal searches, the method has been shown to be backwards stable [Men06, §2.1.2], which was done by combining an upper bound on the accuracy from horizontal searches with a lower bound on the accuracy from vertical searches. Via Theorems 3.1 and 3.4, the extension to computing the spectral value set abscissa is clear, but, as noted in [BLO03, §6], there is one last subtlety that must be addressed to ensure a robust implementation in practice.

Suppose that a given vertical search passes through the interior of a spectral value set such that it intersects its boundary at three points and the resulting vertical cross-section intervals combined with the boundary to the right of them form an outline similar to the capital letter “B”. While the top and bottom boundary points on the vertical line will correspond to simple eigenvalues of (17), the middle boundary point will correspond to a double eigenvalue. Due to rounding error, an eigensolver may only return the upper and lower simple imaginary eigenvalues and fail to return the double imaginary eigenvalue between them. In this case, the algorithm would find a single vertical cross-section interval, instead of the two actual adjacent intervals. If the missed double eigenvalue also happens to coincide with the midpoint of the larger computed interval, the subsequent (and only) horizontal search will not be able to make any rightward progress. Hence, the algorithm will erroneously terminate there, failing to proceed to either of the two locally rightmost points further to the right as it should. Per [BLO03, §6], this pitfall can occur in practice, but remarkably, it can be overcome via a simple fix: split any vertical cross-section into two whenever the previous best horizontal search (i.e. the one that maximizes (18)) passes through it and is considered too close to its midpoint. The previous horizontal

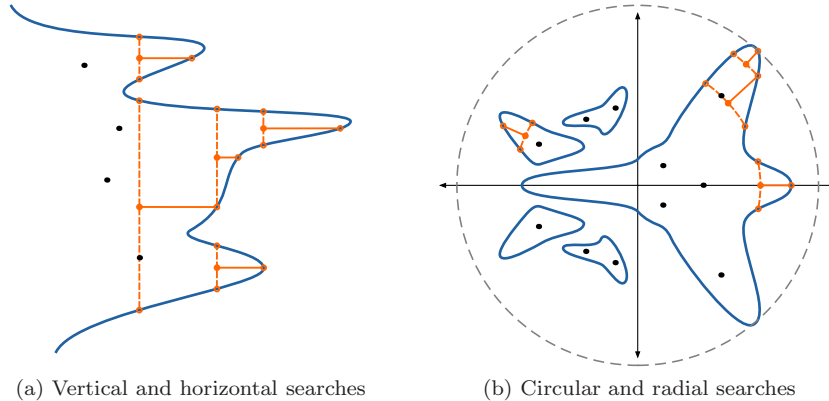


Figure 1: Illustrations of the iterations (shown in orange) of the directly-extended criss-cross methods. The spectrum of (A, E) and the spectral value set boundaries are respectively shown by black dots and blue contours. For the abscissa case (left), the dashed vertical line segments with dots at their midpoints show the cross sections found by the vertical searches, while the solid horizontal line segments depict the horizontal searches rightward. For the radius case (right), the dashed arcs, also with dots at their midpoints, show the results of the circular searches, while the emanating rays depict the radial searches outward; the current best estimate of the spectral value set radius is shown by the grey dashed circle centered at the origin.

search determines the split point and only one interval may be split per vertical search, thus increasing the number of horizontal searches incurred per iteration at most by one.

Remark 3.5. *On [BLO03, p. 373], a second test is described to avoid splitting intervals too frequently (which would increase cost), based on skipping the above safeguard whenever the intervals are deemed sufficiently small. Oddly, this second test is not implemented in the authors' MATLAB routines, although their comments in the code clearly refer to it as well. Robustly implementing such a "bypass" test also seems difficult: given a problem which requires the safeguard to prevent stagnation, the problematic cross-section interval can always be shrunk to any desired length by simply rescaling the entire problem, thus ensuring stagnation for this rescaled problem.*

4 The improved abscissa algorithm

While computing all the imaginary eigenvalues of $(\mathcal{M}_{\gamma x}, \mathcal{N})$, the pencil given by the matrices in (17), can be quite expensive, merely computing the norm of the transfer function can be done much faster. As we reported in [BM18, Table 2], this performance gap ranged from up to 2.47 to 119 times faster for various random dense examples. Thus, there is a potential to increase efficiency by working with the transfer function as opposed to Hamiltonian eigenvalue problems wherever possible. This is particularly so for input-output systems, where $m, p \ll n$ is typical, since computing the eigenvalues of $(\mathcal{M}_{\gamma x}, \mathcal{N})$ is relatively unaffected by dimensions m and p while the norm of the transfer function (a $p \times m$ matrix) becomes significantly cheaper to compute for small m, p . Since obtaining all vertical cross sections on every iteration is necessary to ensure global convergence, which as far as is known, must be done via computing all the eigenvalues of $(\mathcal{M}_{\gamma x}, \mathcal{N})$, we instead focus on avoiding the difficult and expensive eigenvalue problems in the horizontal search phases. As we will see in §9, this approach can be several times faster than the directly-extended method and also reduces numerical inaccuracies due to rounding errors in the eigensolves (see Figure 2).

4.1 Horizontal searches via root finding

Instead of using Theorem 3.4 for horizontal searches, as a first step in exploiting the above cost disparity, we propose to find boundary points further to the right via root finding using the norm of the transfer function. With y specifying a fixed vertical position, we parameterize the largest singular value of the transfer function by the horizontal position x :

$$g_y(x) := \|G(\lambda_y(x))\|_2 = \|CZ_y(x)^{-1}B + D\|_2, \quad (19)$$

where $\lambda_y(x) := x + \mathbf{i}y$ and $Z_y(x) := \lambda_y(x)E - A$. Then, with Ω_k defining a cross section of nonzero length along vertical line $x = \eta$, with midpoint $\eta + \mathbf{i}\psi_k$, the globally rightmost point of $\sigma_\varepsilon(A, B, C, D, E)$ along line $L(0, \psi_k)$ is given by the rightmost root x_\star of

$$g_y(x) - \varepsilon^{-1} = 0, \quad (20)$$

with $x_\star = \omega_l > \eta$. Since (20) may have more than one root to the right of line $x = \eta$, rooting finding will not always guarantee that x_\star is found. However, for η sufficiently close to the value of the ε -spectral value set abscissa, x_\star will be the only remaining root of (20) to the right and so this will not be a problem as the algorithm converges. Furthermore, if we maintain updating lower and upper bounds $x_{\text{lb}} \geq \eta$ and x_{ub} such that (20) is always positive at x_{lb} and always negative at x_{ub} , at least always finding a root $\tilde{x}_\star > \eta$ of (20) in bracket $(x_{\text{lb}}, x_{\text{ub}})$ such that $\tilde{x}_\star + \mathbf{i}\psi_y$ is also a locally rightmost point of $\sigma_\varepsilon(A, B, C, D, E) \cap L(0, \psi_k)$ is guaranteed. This bracketing scheme precludes the obviously suboptimal possibility of converging to a root $\tilde{x}_\star > \eta$ such that $\tilde{x}_\star + \mathbf{i}\psi_y$ is a locally *leftmost* point of $\sigma_\varepsilon(A, B, C, D, E) \cap L(0, \psi_k)$.

While the current horizontal position $x = \eta$ always provides an initial lower bound, an upper bound must be found iteratively but this is always doable; since $\lim_{x \rightarrow \infty} g_y(x) = \|D\|_2$ and $\varepsilon\|D\|_2 < 1$, (20) converges to some negative value as $x \rightarrow \infty$. Furthermore, by exploiting first and possibly second derivatives of singular values, a hybrid Newton- or Halley-based root-finding method enforcing our above bracketing convergence criteria could be employed; near roots of (20), quadratic or cubic convergence would be expected. Since the first and second derivatives of (20) are also relatively cheap to obtain compared to (20) itself (as discussed in §2.2), it stands to reason that computing a root $\tilde{x}_\star > \eta$ may be significantly faster than computing x_\star via Theorem 3.4, at least for all but the smallest of problems.

The first and second derivatives of (19) are as follows. Suppose that $g_y(\hat{x})$ is a simple singular value with associated left and right singular vectors \hat{u} and \hat{v} . As $\lambda'_y(x) = 1$ and $\lambda''_y(x) = 0$, by (13), it follows that

$$(G \circ \lambda_y)'(x) = -CZ_y(x)^{-1}EZ_y(x)^{-1}B \quad (21a)$$

$$(G \circ \lambda_y)''(x) = 2CZ_y(x)^{-1}EZ_y(x)^{-1}EZ_y(x)^{-1}B. \quad (21b)$$

Again by (14), the first derivative of (19) at \hat{x} is

$$g'_y(\hat{x}) = -\text{Re}(\hat{u}^*CZ_y(\hat{x})^{-1}EZ_y(\hat{x})^{-1}B\hat{v}), \quad (22)$$

while its second derivative at \hat{x} can be computed via applying Theorem 2.12 to matrix (15) with first and second derivatives (16), respectively defined by $G(\lambda_y(\hat{x}))$ and the matrix derivatives given in (21) evaluated at \hat{x} .

Remark 4.1. While [BLO03, Theorem 4.1] also considered the pseudospectral analogues of the first derivative given in (22), interestingly it was only used analytically and not computationally to improve efficiency and accuracy, as we do here.

We forgo further root-finding details and instead specify the following abstract function that we will utilize as a subroutine in our improved method.

Definition 4.2. Let $[r, \delta] = \text{findARootToTheRight}(f(\cdot), x_0)$ be some routine that implements the bracketing scheme described above, which given a function $f(\cdot)$ and an initial guess x_0 with $f(x_0) > 0$, returns a root r of $f(\cdot)$ such that $r > x_0$ and $f(r + \mu) < 0$ for all $\mu \in (0, \beta)$ for some fixed value $\beta > 0$. In inexact arithmetic, only $f(r) \approx 0$ is guaranteed and $r + \delta$ would have been the next Newton/Halley iterate.

4.2 Intelligently ordering the horizontal searches

The second way we exploit the increased efficiencies of working with the transfer function is by intelligently ordering the q horizontal searches on each iteration, so that we solve the most promising ones first, i.e., the ones likely to provide the most rightward progress in the spectral value set. Then, provided the predicted ordering is sufficiently accurate, already computed solutions to the more promising root problems can be leveraged to cheaply determine when solving the subsequent root problems is either not necessary or to at least warm start the computations. Our exact procedure works as follows.

Observe that the left side of (20) provides a measure of distance between a point $x + \mathbf{i}y$ and the boundary of $\sigma_\varepsilon(A, B, C, D, E)$. It thus stands to reason that a global optimizer of (18) might most likely lie on the particular horizontal line $\mathbf{i}\psi_k$ that maximizes $g_{x=\eta}(y)$ for $y \in \{\psi_1, \dots, \psi_q\}$. However, we have found that using either

$$N_k = -\frac{g_{y=\psi_k}(\eta) - \varepsilon}{g'_{y=\psi_k}(\eta)} \quad \text{or} \quad H_k = -\frac{2 \cdot g_{y=\psi_k}(\eta) \cdot g'_{y=\psi_k}(\eta)}{2 \cdot [g'_{y=\psi_k}(\eta)]^2 - g_{y=\psi_k}(\eta) \cdot g''_{y=\psi_k}(\eta)}, \quad (23)$$

the initial Newton/Halley steps for each of the horizontal root-finding subproblems, often produces an even better ordering. Before solving any of the root problems for the q horizontal searches, we compute, say H_k , at each of the $\eta + \mathbf{i}\psi_k$ midpoints, and then reorder the searches so that they are in descending order with respect to their H_k values. For convenience, assume that the ψ_k midpoints are already in this order. Let \tilde{x}_* be a computed root of (20) for $y = \psi_1$, which had nothing but η to use as a starting point. We then warm start the second solve, (20) for $y = \psi_2$, using \tilde{x}_* as a starting point. If the left side of (20) is negative at \tilde{x}_* , we immediately have an upper bound on a root for ψ_2 that is worse (to the left) than root \tilde{x}_* for ψ_1 and we have no evidence that there are any other roots to the right; hence, we can completely skip solving (20) for ψ_2 and instead proceed to ψ_3 . Similarly, if the left side of (20) is exactly zero at \tilde{x}_* , then (20) is already solved but does not yield a better root so we again proceed to ψ_3 without further computation. However, if the left side of (20) for ψ_2 is positive, then solving (20) for ψ_2 initialized at \tilde{x}_* must yield a root $\hat{x}_* > \tilde{x}_*$, and so the solve should proceed. We continue to warm start the subsequent subproblems with the current best root, a clearly better strategy than solving them all initialized at $x = \eta$.

Finally, if the rightmost computed approximate root of (20) ends up corresponding to a point just inside the spectral value set, we slightly perturb it so that it is just outside, by adding a multiple of the final Newton/Halley step. This slight modification prevents the algorithm from incurring two vertical searches just before termination when only one is necessary numerically. The full pseudocode is given in Subroutine 1. While we have not used parallelism in our description, it could potentially further improve running times.

4.3 The complete improved abscissa algorithm

Naturally, we advocate using `fastSearch` (Subroutine 1) in lieu of the earlier expensive eigenvalue-based horizontal searches. However, we also propose one last but simple modification: to start with a horizontal search rather than a vertical one. This has two benefits. First, it often reduces the total number of horizontal searches incurred. The number of vertical cross sections generally decreases as $\eta \rightarrow \eta_*$ and since there can be up to n cross sections, which is more likely when

Subroutine 1 $[x, \psi] = \text{fastSearch}(\eta_0, \{\psi_1, \dots, \psi_q\})$

Input:

$\eta_0 \in \mathbb{R}$, an initial lower bound
 $\{\psi_1, \dots, \psi_q\}$ with each $\psi_k \in \mathbb{R}$

Output:

$x > \eta$, the rightmost root *encountered* of (20) over $y \in \{\psi_1, \dots, \psi_q\}$ or $\eta = \eta_0$

```

1: compute the initial Newton (or Halley) steps  $\{N_1, \dots, N_q\}$  using (23)
2: let  $\{\psi_1, \dots, \psi_q\}$  be ordered such that  $N_k$  is decreasing with respect to all  $k$ 
3:  $x := \eta_0$ ;  $\psi := []$ ;  $\delta := []$ 
4: for  $k = 1, \dots, q$  do
5:   set function handle  $f(\cdot) := g_{y=\psi_k}(\cdot) - \varepsilon^{-1}$  // (20) defined for  $y = \psi_k$ 
6:   if  $f(x) > 0$  then
7:      $[x, \delta] := \text{findARootToTheRight}(f(\cdot), x)$ 
8:      $\psi := \psi_k$ 
9:   end if
10: end for
11: // Ensure computed (approximate) rightmost root is not just inside the interior
12: if  $\delta$  is not  $[]$  and  $f(x) > 0$  then
13:    $\delta := \min\{|\delta|, |x| \cdot \epsilon_{\text{mach}}\}$  // Make sure  $x + \delta > x$  holds to machine precision
14:    $x := \min\{x + k\delta : f(x + k\delta) \leq 0 \text{ for } k \in \{1, 2, \dots\}\}$ 
15: end if

```

$\eta \ll \eta_*$, the reduction in horizontal searches can be dramatic (though our `fastSearch` subroutine generally only resolves at most a handful of roots when given many searches). Moreover, by having a better (larger) initial estimate of η_* , the number of vertical searches may also be reduced. While most of our efficiency gains will be from `fastSearch`, this additional change also has non-negligible effect (see Table 1 in §9). The second benefit is that it eliminates the need for an ad hoc perturbation to do the first vertical search just to the right of an eigenvalue (A, E) , since doing it through an eigenvalue would violate the assumptions of Theorem 3.1. Initialization is typically done from a controllable and observable eigenvalue of (A, E) ; in practice, it is best to provide a minimal realization as input. Pseudocode for the complete improved method is given in Algorithm 1.

5 Directly extending the pseudospectral radius algorithm

We now describe and directly extend the pseudospectral radius method of [MO05] to the spectral value set radius, by generalizing its alternating circular and radial search phases. Although respectively analogous to the vertical and horizontal searches described in §3, a key difference here is that circular searches may sometimes fail, either because the corresponding pencils are singular or the searches do not intersect with the spectral value set boundary. For now, we assume neither of these happen.

5.1 Circular search

We now give an analogue of Theorem 3.1 that relates singular values of the norm transfer function evaluated at points on a chosen circle of radius $r > 0$ centered at the origin with unimodular eigenvalues of an associated symplectic pencil. Less general versions of this result go back as

Algorithm 1 $[\eta] = \text{svsAbscissa}(\varepsilon, A, B, C, D, E)$

Input:

$\varepsilon > 0$ with $\varepsilon \|D\|_2 < 1$ and matrices A, B, C, D, E defining $\sigma_\varepsilon(A, B, C, D, E)$

Output:

η , the computed value of $\alpha_\varepsilon(A, B, C, D, E)$

```

1:  $\Lambda := \text{eig}(A, E)$ 
2:  $\Lambda := \{\lambda \in \Lambda : \lambda \text{ meets user's inclusion criteria: controllable/observable}\}$ 
3: if  $\infty \in \Lambda$  then
4:   return  $\eta = \infty$ 
5: end if
6:  $\lambda_0 := \arg \max\{\text{Re } \lambda : \lambda \in \Lambda\}$ 
7: // More efficient to start with a horizontal search instead of a vertical one:
8:  $[\eta, y] := \text{fastSearch}(\text{Re } \lambda_0, \{\text{Im } \lambda_0\})$ 
9: while  $\eta < \alpha_\varepsilon(A, B, C, D, E)$  do
10:  compute imaginary eigenvalues  $\{\mathbf{i}y_1, \dots, \mathbf{i}y_l\}$  of (17) for  $x = \eta$  and  $\gamma = \varepsilon^{-1}$ 
11:  form all intervals  $\Omega_k = [y_k, y_{k+1}]$  s.t.  $\eta + \mathbf{i}y \in \sigma_\varepsilon(A, B, C, D, E) \forall y \in \Omega_k$ 
12:   $\Psi := \{\psi_1, \dots, \psi_q\}$  such that  $\psi_k$  is a midpoint of interval  $\Omega_k$ 
13:   $[\eta, y] := \text{fastSearch}(\eta, \Psi)$ 
14: end while

```

far as [HS91, §3], for the special case of fixed radius $r = 1$, $D = 0$, and $E = I$. Similarly to Theorem 3.1, we defer the proof to Appendix A.

Theorem 5.1. *Let $r > 0$ be the radius of a circle centered at the origin, angle $\theta \in [0, 2\pi)$, $\gamma > 0$ not a singular value of D , and $\lambda E - A$ be regular. Consider the matrix pencil $(\mathcal{S}_{\gamma r}, \mathcal{T}_{\gamma r})$, where*

$$\begin{aligned} \mathcal{S}_{\gamma r} &:= \begin{bmatrix} A - BR^{-1}D^*C & -\gamma BR^{-1}B^* \\ 0 & rE^* \end{bmatrix}, \\ \mathcal{T}_{\gamma r} &:= \begin{bmatrix} rE & 0 \\ -\gamma C^*S^{-1}C & A^* - C^*DR^{-1}B^* \end{bmatrix}, \end{aligned} \tag{24}$$

$R = D^*D - \gamma^2 I$ and $S = DD^* - \gamma^2 I$. Then $e^{\mathbf{i}\theta}$ is an eigenvalue of $(\mathcal{S}_{\gamma r}, \mathcal{T}_{\gamma r})$ if and only if γ is a singular value of $G(re^{\mathbf{i}\theta})$ and $re^{\mathbf{i}\theta}$ is not an eigenvalue of (A, E) .

Setting $\gamma = \varepsilon^{-1}$, Theorem 5.1 provides a means to compute all the boundary points, if any, of an ε -spectral value set that lie on any desired circle of radius r centered at the origin. More specifically, let $\{\theta_1, \dots, \theta_l\}$ be the set of angles, all in $[0, 2\pi)$ and sorted in increasing order, given by the (we assume nonempty) set of unit-modulus eigenvalues of (24). Thus, each point $re^{\mathbf{i}\theta_j}$ is a boundary point of $\sigma_\varepsilon(A, B, C, D, E)$. As in §3.1, determining the subset of arcs on the circle of radius r that pass through the spectral value set can be reliably done by just evaluating the norm of the transfer function at the midpoints of all the candidate arc segments given by $\Omega_k = [\theta_k, \theta_{k+1}]$ for $k = 1, \dots, l-1$, but now the additional “wrap-around” interval $[\theta_l, \theta_1 + 2\pi]$ must be also be considered.

5.2 Radial search

Given a circle of radius $r = \eta$, let $\Omega_k = [\theta_k, \theta_{k+1}]$ denote a non-zero length arc of this circle which also lies in $\sigma_\varepsilon(A, B, C, D, E)$ and $\Omega = \{\Omega_1, \dots, \Omega_q\}$ denote the set of all such arcs. Similar to the abscissa case, [MO05] proposed to make outward progress by taking the midpoints of these arc

segments, i.e. $\psi_k = 0.5(\theta_k + \theta_{k+1})$, as directions of rays from the origin on which to find more distant boundary points. The maximal outward progress is then:

$$\max_{\Omega_k \in \Omega} \max\{|\lambda| : \lambda \in \sigma_\varepsilon(A, B, C, D, E) \text{ and } \text{Arg } \lambda = \psi_k\}, \quad (25)$$

which can be solved by applying Theorem 3.4 to each of the lines $L(\psi_k, 0)$ and taking the outermost of all the computed boundary points. Of course, we will instead adapt our new faster `fastSearch` subroutine; see §6.

5.3 The complete directly-extended radius algorithm

The method of [MO05] alternates between radial and circular searches to respectively increase estimate $r = \eta$ (monotonically) and find new arc-shaped cross sections of the pseudospectrum. A robust implementation also requires the splitting safeguard described at the end of §3.3. It converges to a globally outermost point λ_* of $\sigma_\varepsilon(A)$ with $\eta_* = |\lambda_*| = \rho_\varepsilon(A)$, with a local quadratic convergence rate [MO05, §2.4]; a sample of the iterations is depicted visually in Figure 1b. However, global convergence is not just predicated upon initializing the algorithm with an initial radius $r \geq \rho(A)$; the method must also handle the aforementioned possibility of circular searches failing. This problem was dealt with in [MO05, §2.5] in the following manner. We first present respective generalizations of [MO05, Theorem 2.11 and Corollary 2.12]; the proofs extend directly via simple substitutions.

Theorem 5.2. *Given some $r > 0$, if the matrix pencil defined by (24) is singular and the largest singular value of $G(re^{i\theta})$ is simple for all $\theta \in [0, 2\pi)$, then either:*

1. *the boundary of $\sigma_\varepsilon(A, B, C, D, E)$ contains the circle of radius r or*
2. *the circle of radius r is strictly inside $\sigma_\varepsilon(A, B, C, D, E)$.*

Corollary 5.3. *Suppose that for some fixed $r > 0$, $\|G(re^{i\theta})\|_2 - \varepsilon^{-1} < 0$ holds for at least one angle $\theta \in [0, 2\pi)$. Then the matrix pencil defined by (24) is regular.*

First, [MO05] proposed starting the algorithm with a single radial search along the ray from the origin through a globally rightmost eigenvalue λ_0 of A . By applying Theorem 3.4 to find λ_{bd} , a globally outermost point of $\sigma_\varepsilon(A) \cap L(\text{Arg } \lambda_0, 0)$ or the solution of (25) in the direction of λ_0 , Corollary 5.3 asserts that the matrix pencil given by (24) is regular for all $r > |\lambda_{\text{bd}}|$. Moreover, since the corresponding circular searches must then always have portions outside of $\sigma_\varepsilon(A)$, they are also guaranteed not to be problematic interior searches. However, in exact arithmetic, the possibility of an initial circular search with radius $|\lambda_{\text{bd}}|$ corresponding to a singular pencil cannot be ruled out. Furthermore, the computed version of λ_{bd} , which we denote $\tilde{\lambda}_{\text{bd}}$, may be strictly inside $\sigma_\varepsilon(A)$ and so the possibility that a circular search of radius $|\tilde{\lambda}_{\text{bd}}|$ does not intersect with the pseudospectral boundary cannot be ruled out either. Thus, [MO05] also proposed potentially increasing the radius of the very first circular search from $|\tilde{\lambda}_{\text{bd}}|$ to $|\tilde{\lambda}_{\text{bd}}| + k\delta_0$, where δ_0 is the initial Newton step to change the magnitude of $\tilde{\lambda}_{\text{bd}}$ in order to move it to the pseudospectral boundary and k is the smallest nonnegative integer such that adding $k\delta_0$ to its magnitude indeed puts the resulting point outside of $\sigma_\varepsilon(A)$. When $\tilde{\lambda}_{\text{bd}}$ is strictly inside the pseudospectrum, $\delta_0 > 0$ holds and the authors noted that small k (e.g. 1 or 2) typically sufficed to move $\tilde{\lambda}_{\text{bd}}$ outside; otherwise $k = 0$ is taken.² By Corollary 5.3, it is not necessary to perturb any subsequent circular searches but there is a caveat. If the perturbation is too small the resulting pencil may be *nearly* singular and thus still problematic to solve (which we have observed in practice), or alternatively, the perturbation is large but then accuracy may be sacrificed. While this procedure extends to the directly-extended spectral value set radius algorithm, it does not for our improved radius algorithm.

²In fact, this is essentially the same perturbation procedure we have employed at the end of `fastSearch` but motivated by very different reasons.

Remark 5.4. In [MO05], starting with a radial search only seems to be for avoiding singular pencils; no mention is made that it can also have efficiency benefits.

6 The improved radius algorithm

Before describing `fastSearch` for the radial phases, to efficiently find locally-optimal solutions of (25), note that the loss of global optimality in these searches violates the necessary assumptions to use the existing technique of [MO05] for handling singular pencils and/or interior circular searches. We now adapt `fastSearch` and then propose a new compatible technique to overcome such difficult pencils/searches.

6.1 Adapting `fastSearch` for the radial phase

Parameterizing the largest singular value of the transfer function in polar coordinates, with varying radius r for a fixed angle θ , yields

$$g_\theta(r) := \|G(\lambda_\theta(r))\|_2 = \|CZ_\theta(r)^{-1}B + D\|_2, \quad (26)$$

where $\lambda_\theta(r) := re^{i\theta}$ and $Z_\theta(r) := \lambda_\theta(r)E - A$. Hence each outward search along a ray in direction θ is done by finding a root of

$$g_\theta(r) - \varepsilon^{-1} = 0. \quad (27)$$

The first and second derivatives of (26) are as follows. Assume that $g_\theta(\hat{r})$ is a simple singular value, with left and right singular vectors \hat{u} and \hat{v} . As $\lambda'_\theta(r) = e^{i\theta}$ and $\lambda''_\theta(r) = 0$, by (13), it follows that

$$(G \circ \lambda_\theta)'(r) = -e^{i\theta} CZ_\theta(r)^{-1} E Z_\theta(r)^{-1} B \quad (28a)$$

$$(G \circ \lambda_\theta)''(r) = 2e^{2i\theta} CZ_\theta(r)^{-1} E Z_\theta(r)^{-1} E Z_\theta(r)^{-1} B, \quad (28b)$$

and so by (14), the first derivative of (26) at \hat{r} is

$$g'_\theta(\hat{r}) = -\operatorname{Re}(e^{i\theta} \hat{u}^* CZ_\theta(\hat{r})^{-1} E Z_\theta(\hat{r})^{-1} B \hat{v}). \quad (29)$$

Using (28), the second derivative of (26) at \hat{r} can be computed via Theorem 2.12. The subproblems given by (27) are prioritized in descending order with respect to their initial Newton/Halley steps, i.e. (23) with $g_{y=\psi_k}(\eta)$ replaced by $g_{\theta=\psi_k}(\eta)$. Thus remaining modification to `fastSearch` replaces (20) with (27) in Subroutine 1.

Remark 6.1. Similar to [BLO03], the pseudospectral analogue of the first derivative given in (29) was considered in [MO05, Theorem 2.3], but it too was not used computationally to improve efficiency, as we do here.

6.2 A new method for handling singular pencils and interior searches

Although `fastSearch` is guaranteed to converge to a global solution of (25) for η sufficiently close to η_* , it may only return locally-optimal solutions for smaller values of η . Consequently, and in contrast to the directly-extended algorithm, we cannot rule out the possibility of encountering a (nearly) singular pencil or problematic interior search on *any* iteration. It might seem tempting to just apply the perturbation technique of [MO05] to every iteration, but this comes with the accuracy-versus-reliability tradeoff mentioned above. However, since `fastSearch` finds boundary points to high accuracy, δ_0 will generally be tiny, meaning that using the earlier singular pencil procedure of [MO05] would almost always result in pencils that are still nearly singular. The technique of [MO05] is reasonable for the directly-extended algorithm because a) its δ_0 value is generally much larger due to the relatively higher inaccuracy of obtaining the solution to (25) via

computing eigenvalues (Figure 2 demonstrates such errors) and b) it is only needed once rather than multiple times (where the chance of encountering a single failure increases significantly). Faced with such difficulties, we consider an entirely new approach, using the following new result.

Theorem 6.2. *Given $\varepsilon > 0$ with $\varepsilon\|D\|_2 < 1$, set $\gamma = \varepsilon^{-1}$ and let η be such that the circle of radius η centered at the origin both encircles all the eigenvalues of (A, E) and is strictly in the interior of $\sigma_\varepsilon(A, B, C, D, E)$. Let $\delta > 0$ be the largest value such that, for all $t \in [0, 1]$, circles of radius $\eta + t\delta$ are still subsets of $\sigma_\varepsilon(A, B, C, D, E)$. Finally, let $R = \{r_1, \dots, r_l\}$ denote the subset of positive radii corresponding to the boundary points of $\sigma_\varepsilon(A, B, C, D, E)$ that lie on $L(\theta, 0)$ but are outside the circle of radius η , where $\theta \in [0, 2\pi)$ has been chosen randomly. Then for $\hat{r} = \min\{r_1, \dots, r_l\} > \eta$, either of the two following scenarios may hold:*

1. $(\mathcal{S}_{\gamma r}, \mathcal{T}_{\gamma r})$ is singular for $r = \eta + \delta$ but $\hat{r} = \eta + \delta = \rho_\varepsilon(A, B, C, D, E)$ or
2. $(\mathcal{S}_{\gamma r}, \mathcal{T}_{\gamma r})$ is regular for $r = \eta + \delta$ and, with probability one, $\hat{r} > \eta + \delta$.

Proof. We first consider the case where $(\mathcal{S}_{\gamma r}, \mathcal{T}_{\gamma r})$ is singular at $r = \eta + \delta$. Since $\eta + \delta \in R$, it must be that $re^{i\theta}$ is a boundary point of $\sigma_\varepsilon(A, B, C, D, E)$, and by Theorem 5.2, the circle of radius r centered at the origin must be a subset of the boundary of $\sigma_\varepsilon(A, B, C, D, E)$. Furthermore, $\rho_\varepsilon(A, B, C, D, E) \geq r$. If strict inequality holds, then there must exist some boundary point $\hat{\lambda} \in \sigma_\varepsilon(A, B, C, D, E)$ with $|\hat{\lambda}| > r$. But this contradicts the conclusion of Lemma 2.6, that there exists a path taking some controllable and observable eigenvalue of (A, E) to $\hat{\lambda}$ such that only $\lambda(1) = \hat{\lambda}$ is a boundary point, since any such $\lambda(t)$ must also cross the circle of radius r at some $t < 1$. Hence, $r = \hat{r}$ as R only contains a single unique value, namely $\eta + \delta$.

Now suppose $(\mathcal{S}_{\gamma r}, \mathcal{T}_{\gamma r})$ is regular at $r = \eta + \delta$. By assumption, the circle of radius $\eta + \delta$ only touches the spectral value boundary but does not cross it. Furthermore, since the pencil is regular, by Theorem 5.1, there can only be a finite number (at most n) of contact points between this circle and the spectral value set boundary. Suppose that $\hat{r} = \eta + \delta$, noting that by assumption, \hat{r} cannot be any smaller. Then, for boundary point $\hat{r}e^{i\theta}$, its angle θ must be equal to one of the angles corresponding to the finite set of contact points. As $\theta \in [0, 2\pi)$ was chosen randomly, the probability of this event occurring is zero. Therefore, with probability one, θ will not correspond to any of the contact points on the circle of radius $\eta + \delta$ and thus, $\hat{r} > \eta + \delta$. \square

Theorem 6.2 clarifies what to do when **fastSearch** returns a point $\tilde{\lambda}_{\text{bd}}$ with $|\tilde{\lambda}_{\text{bd}}| = \eta$ such that, due to rounding error, $\tilde{\lambda}_{\text{bd}}$ is distance δ inside $\sigma_\varepsilon(A, B, C, D, E)$ and the subsequent circular search for $r = \eta$ returns no arc cross sections. Either the algorithm has actually converged to $\rho_\varepsilon(A, B, C, D, E)$ within the numerical limits of the root-finding method itself or, by reapplying **fastSearch** in a random direction given by $\theta \in [0, 2\pi)$ through interior point $\eta e^{i\theta}$, the algorithm can, with probability one, obtain a new more distant point beyond the current problematic local area involving singular pencils and/or interior searches. Put more simply, problematic circular searches encountered on any iteration can be overcome by applying **fastSearch** in one or more random directions and if the algorithm still converges to a singular pencil, then with probability one it has also converged to $\rho_\varepsilon(A, B, C, D, E)$.

6.3 The complete improved radius algorithm

Like our improved abscissa method, the improved radius algorithm uses **fastSearch** but now adapted for the radial searches. It starts with a single initial radial search outward, from an outermost eigenvalue of (A, E) (typically controllable and observable), and then alternates between circular and radial searches. However, whenever a circular search does not return any arc cross sections of $\sigma_\varepsilon(A, B, C, D, E)$, which generally would be a sign of convergence, the new algorithm must also consider the possibility that the search simply failed. Thus, whenever no arc cross sections are obtained, the improved algorithm simply applies **fastSearch** in one or more randomly chosen directions in $[0, 2\pi)$ to distinguish between convergence and encountering interior searches

Algorithm 2 $[\eta] = \text{svsRadius}(\varepsilon, A, B, C, D, E)$

Input:

$\varepsilon > 0$ with $\varepsilon \|D\|_2 < 1$ and matrices A, B, C, D, E defining $\sigma_\varepsilon(A, B, C, D, E)$
 r a positive integer, specifying how many random angles to try

Output:

η , the computed value of $\rho_\varepsilon(A, B, C, D, E)$, with probability one

```

1:  $\Lambda := \text{eig}(A, E)$ 
2:  $\Lambda := \{\lambda \in \Lambda : \lambda \text{ meets user's inclusion criteria: controllable/observable}\}$ 
3: if  $\infty \in \Lambda$  then
4:   return  $\eta = \infty$ 
5: end if
6:  $\lambda_0 := \arg \max\{|\lambda| : \lambda \in \Lambda\}$ 
7:  $\Psi := \{\text{Arg } \lambda_0, \psi_1, \dots, \psi_r\}$  such that  $\psi_k$  is chosen randomly from  $[0, 2\pi)$ 
8:  $[\eta, \theta] := \text{fastSearch}(|\lambda_0|, \Psi)$ 
9: while  $\eta < \alpha_\varepsilon(A, B, C, D, E)$  do
10:  compute unimodular eigenvalues  $\{e^{i\theta_1}, \dots, e^{i\theta_l}\}$  of (24) for  $r = \eta$  and  $\gamma = \varepsilon^{-1}$ 
11:  form all intervals  $\Omega_k = [\theta_k, \theta_{k+1}]$  s.t.  $\eta e^{i\theta} \in \sigma_\varepsilon(A, B, C, D, E) \forall \theta \in \Omega_k$ 
12:  if no such intervals then
13:     $\Psi := \{\psi_1, \dots, \psi_r\}$  such that  $\psi_k$  is chosen randomly from  $[0, 2\pi)$ 
14:  else
15:     $\Psi := \{\psi_1, \dots, \psi_q\}$  such that  $\psi_k$  is a midpoint of interval  $\Omega_k$ 
16:  end if
17:   $[\eta, \theta] := \text{fastSearch}(\eta, \Psi)$ 
18: end while

```

or (nearly) singular pencils. If the algorithm has indeed converged, calling `fastSearch` has no effect, except for the relatively small additional cost to evaluate the norm of the transfer function at a handful of random points. If the algorithm has not converged, then by Theorem 6.2, with probability one the method is guaranteed to increase its current estimate of $\rho_\varepsilon(A, B, C, D, E)$ beyond the problematic region. Furthermore, as long as *any* outward progress is being made, `fastSearch` will continued to be called with new random directions every iteration until either a subsequent circular search returns one or more arc cross sections or `fastSearch` can no longer increase the radius estimate at all. This allows the algorithm to robustly push past problematic regions where successive circular searches may fail to return any arcs. However, we have observed that typically only a single attempt is necessary in practice. Pseudocode for the complete improved radius method is given in Algorithm 2.

7 Global Convergence

We give the following proof of convergence, which is simpler and less technical than those given in [BLO03] and [MO05].

Theorem 7.1. *Algorithms 1 and 2 converge to the ε -spectral value set abscissa and radius, respectively.*

Proof. Let η_\star be the value of the ε -spectral value set abscissa/radius, attained at some non-isolated globally rightmost (outermost) point λ_\star , and $\{\eta_k\}$ be the sequence our methods generate, which by construction must be monotonically increasing and $\eta_k \leq \eta_\star$ must hold. Let $\lambda(t)$ be

one of the continuous paths, specified by Lemma 2.6, taking an eigenvalue of (A, E) to λ_* with $\mathcal{N}(t) \subset \sigma_\varepsilon(A, B, C, D, E)$ a neighborhood of $\lambda(t)$ of radius $\delta(t) > 0$ for all $t \in [0, 1)$. Setting $f(t) = \operatorname{Re} \lambda(t)$ ($f(t) = |\lambda(t)|$), there exists $t_0 \in [0, 1)$ such that $f(t_0) = \eta_0$. So suppose that $\eta_k \rightarrow \hat{\eta} < \eta_*$. By Theorem 6.2, encountering singular pencils can be ruled out since this only occurs in the radius case when $\hat{\eta} = \eta_*$. Let $\Omega(\eta)$ denote the set of intervals corresponding to vertical (circular) cross sections varying by $x = \eta$ ($r = \eta$) and consider:

$$l(\eta) := \max_{\Omega_k \in \Omega(\eta)} \{|\omega_{k+1} - \omega_k| : \Omega_k = [\omega_k, \omega_{k+1}]\}.$$

As singular pencils are excluded, by continuity of eigenvalues, $l(\eta)$ must be continuous on $[\eta_0, \hat{\eta}]$. Given the (possibly disjoint) subset $D \subset [t_0, 1)$ where $f(t)$ is strictly increasing, there exists $\hat{t} \in D$ such that $f(\hat{t}) = \hat{\eta}$. Thus $l(f(t)) \geq \delta(t) > 0$ holds for all $t \in D$ and $l(\eta) \not\rightarrow 0$ as $\eta \rightarrow \hat{\eta}$. This implies continuous convergence to a cross section of positive length at $\hat{\eta}$, whose midpoint must of course be strictly in the interior of the spectral value set. Hence, the methods cannot stagnate at $\hat{\eta}$. \square

8 Implementation

We implemented Algorithms 1 and 2 in a single new MATLAB routine called `specValSet`, which is publicly available as part of the open-source library ROSTAPACK: RObust STAbility PACKage, starting with the v2.0 release.³ For the radius case, whenever no intervals are obtained, `specValSet` generates three random angles for `fastSearch` for invoking Theorem 6.2. By default, all evaluations of the norm of the transfer function are done using the Hessenberg factorization techniques of [Lau81, VDV85] mentioned at the end of §2.2, though `specValSet` also supports using LU factorizations.

An evaluation of which bracketing and root-finding method would be most efficient to use for implementing the prerequisite subroutine `findARootToTheRight` (specified in Definition 4.2) is beyond the scope of this article. We implemented a second-order version of `findARootToTheRight`. It first brackets a root by iteratively increasing the current guess by adding the larger of either two times the absolute value of the Halley step or the distance from the current guess and the initial guess x_0 , until an upper bound has been found (while increasing the lower bound along the way). Then it computes a root using a hybrid Halley's method with our bracketing. We found that this was generally more efficient than using first-order schemes. The very first step of the upper bound search increases the initial guess by at least $\max\{10^{-6}, 0.01|x_0|\}$. If the function given to `findARootToTheRight` fails to return a finite value, our code simply updates the lower bound and increases the current guess.

As a practical optimization, for when all the matrices are real valued but λ_0 is not, `specValSet` always attempts to first find a root along the x -axis, either to the right of λ_0 (or outward in either direction for the ε -spectral value set radius) before computing a solution to the root problem for λ_0 . Assuming such a root exists along the x -axis, the initial ε -spectral value set abscissa (or radius) estimate η will be increased, from $\eta = \alpha(A, E)$ (or $\eta = \rho(A, E)$) to some larger value corresponding to a boundary point $\sigma_\varepsilon(A, B, C, D, E)$ on the x -axis. Even though this strategy potentially introduces an additional horizontal search (or two radial searches), it often substantially reduces the overall number of *complex-valued* SVDs incurred, replacing them with *much cheaper real-valued ones*. This optimization can have a significant net benefit in terms of running time because it can sometimes require many iterations to find an upper bound for the root-finding problem for λ_0 , which without this optimization, would be initialized at λ_0 , a pole of the transfer function.

The `specValSet` routine has the following similarities to the `pspa` and `pspr` routines of [MO], the respective implementations of the original criss-cross type methods for computing the

³ <http://timitchell.com/software/ROSTAPACK>

pseudospectral abscissa [BLO03] and the pseudospectral radius [MO05]. First, if the problem is real valued, the spectral value sets are symmetric with respect to the x -axis; in this case, any interval $\Omega_k \in \Omega$ that corresponds to a section in the open lower half-plane is discarded (since it is “duplicated” by its positive conjugate). Second, as `pspr` does not use a structure-preserving eigensolver, we used `eig` from MATLAB for all codes in the benchmarks done here; note that any robust implementation should use structure-preserving eigensolvers, such as those available in SLICOT [BMS+99]. Third, `specValSet` simply terminates when the ε -spectral value set abscissa/radius estimate η can no longer be increased, by any amount; no tolerance is needed.

9 Numerical experiments

All experiments were done in MATLAB R2017b on a laptop with an Intel i7-6567U dual-core CPU, 16GB of RAM, and macOS v10.14. Running times were measured using `tic` and `toc`; to account for variability, we report the average time of five trials for each method-problem pair. For `specValSet`, we used ROSTAPACK v2.2 and set `rng(100)` before each trial (as it uses random numbers).

9.1 Spectral value set evaluation

We used 15 publicly-available spectral value set test examples of varying dimensions: four problems (CBM, CM3, CM4, CSE2) from [GGO13] and another 11 from the SLICOT benchmark examples.⁴ Since some of the examples have nonzero D matrices, and $\varepsilon\|D\|_2 < 1$ must hold, we instead calculated specific per-problem values of ε as follows. We computed the continuous- and discrete-time \mathcal{L}_∞ norms for each example, via `getPeakGain` with a tolerance of 10^{-14} , to be respectively used for the ε -spectral value set abscissa and radius evaluations. Let γ_\star denote the corresponding computed \mathcal{L}_∞ -norm value, for either the abscissa or radius case. We then set $\varepsilon := 2\gamma_\star$, provided that γ_\star was a finite positive value and $\varepsilon\|D\|_2 < 0.5$ held. Otherwise, for problems with nonzero D matrices, we used $\varepsilon := 0.5\|D\|_2^{-1}$ and $\varepsilon := 0.01$ for the rest. Each problem was initialized at a rightmost/outermost controllable and observable eigenvalue of (A, E) .

As our improved methods are the first to be able to compute the ε -spectral value set abscissa and radius, there are no other available codes for comparison. Instead, we compared against our own implementations of the directly-extended (DE) variants described in §3 and §5 in order to show the benefits of our modifications. While the values computed by both variants generally agreed with each other, there were three examples, all abscissa problems, where the DE methods incurred relative errors greater than 10^{-10} in magnitude; these are marked with asterisks in Table 1. Before analyzing these errors, we first present the performance results.

For the ε -spectral value set abscissa tests, shown in Table 1, we compared against two versions of the DE approach: one using a vertical search first and an alternative using an initial horizontal search, though we only provide detailed per-problem performance statistics for the former. Overall, our method was much faster than the DE variant using a vertical search first: on average, our method was 321% faster and up to 733% faster (on `eady`). In fact, our new approach was fastest on all 15 problems, all by significant margins; even on CSE2, where performance difference was smallest, the DE variant required about twice as much time. Compared to the DE variant using an initial horizontal search, our new approach was still 254% faster on average, underscoring that the majority of acceleration achieved is due to our new root-finding-based method and not just the simple (though beneficial) idea of starting with a horizontal search.

In Table 2, the corresponding experiments are shown for the ε -spectral value set radius tests. Again our method was fastest on all 15 test problems; on average it was 139% faster than the DE variant and up to 614% faster (on `tline`). However, on `eady`, and `fom`, the performance gains were rather small (14% and 24% faster, respectively). The less pronounced performance gains

⁴ Available at <http://slicot.org/20-site/126-benchmark-examples-for-model-reduction>

Spectral Value Set Abscissa: directly extended versus new method														
Problem	Dimensions			# solves				# searches			time (sec.)	% faster		
	n	m	p	Eig		SVD		vert.		horz.				
build	48	1	1	19	4	25	57	6	4	13	4(4)	0.113	0.049	132
CSE2	63	1	32	5	1	2	10	3	1	2	1(2)	0.047	0.024	99
pde	84	1	1	5	1	2	8	3	1	2	1(2)	0.105	0.034	210
CDplayer	120	2	2	10	3	13	36	4	3	6	3(4)	0.252	0.086	192
CM3	123	1	3	6	2	8	64	3	2	3	2(2)	0.253	0.106	139
heat-cont	200	1	1	5	1	2	33	3	1	2	1(1)	0.552	0.091	504
heat-disc	200	1	1	5	1	2	8	3	1	2	1(1)	0.972	0.190	410
random*	200	1	1	6	2	8	87	3	2	3	2(2)	0.664	0.279	138
CM4	243	1	3	10	2	17	48	3	2	7	2(2)	1.785	0.304	487
tline*	256	2	2	9	2	11	33	3	2	6	2(2)	6.377	1.722	270
iss	270	3	3	6	4	7	47	2	4	4	4(5)	1.565	0.675	132
beam*	348	1	1	9	2	12	25	4	2	5	2(2)	3.157	0.481	556
CBM	351	1	2	8	3	12	63	3	3	5	4(5)	2.978	0.913	226
eady	598	1	1	7	1	5	7	3	1	4	1(2)	8.221	0.987	733
fom	1006	1	1	12	3	15	31	4	3	8	4(6)	61.139	8.852	591
Totals:				122	32	141	557	Average % faster:			321			
(Directly extended with horz. search first)				Average % faster:			254							

Table 1: For each pair of columns, performance data is given for the directly-extended (DE) approach (left) and our improved approach (right) for computing the spectral value set abscissa. Problems marked with asterisks denote where the DE variant had relative errors greater than 10^{-10} . The “Eig” column gives the total number of $2n \times 2n$ eigensolves computed, while the “SVD” column gives the total number of evaluations of the norm of the transfer function. The number of vertical and horizontal searches are given under the “vert.” and “horz.” headers, respectively; for our new method, if the total number of “horz.” searches was greater than the number that *actually needed to be solved*, the latter is given first, with the former given in parenthesis. The time for the faster of the two methods is in bold. Positive percentages in the “% faster” column indicate the amount faster our new method was compared to the DE variant while negative ones indicate the amount faster the DE variant was. The last row gives the average of the % faster values for a second version of DE that starts with a horizontal search instead of a vertical one.

against the DE variant on the radius problems seem to be due to the fact that, on average, the DE variant converged in fewer iterations for the radius case than it did for the abscissa case.

Returning to the three abscissa problems where the DE variants had the highest errors, all were caused by rounding errors when computing the imaginary eigenvalues in the eig-based horizontal and/or vertical searches. On both `beam` and `random` (1.19×10^{-9} and 1.60×10^{-9} relative errors, respectively), rounding errors in computing imaginary eigenvalues for the final horizontal search caused the computed abscissa values to be slightly too large. In contrast, the relative error of -2.38×10^{-8} on `tline` was due to rounding errors in both the horizontal and vertical searches. On the last horizontal search, rounding errors in the computed imaginary eigenvalues caused the computed boundary point to be slightly inside the spectral value set. Another vertical search was then attempted but failed to return any boundary points, again due to rounding errors in computing the imaginary eigenvalues. Hence, the DE variant stopped a bit short of the spectral value set abscissa. This particular failure underscores the importance of using structure-preserving eigensolvers for the vertical (and circular searches), even with our more numerically reliable root-finding-based approach. However, as we will see in §9.2, even structure-preserving eigensolvers are not a panacea for the numerical issues that can arise in

Spectral Value Set Radius: directly extended versus new method														
Problem	Dimensions			# solves				# searches			time (sec.)	% faster		
	n	m	p	Eig		SVD		circ.		rad.				
build	48	1	1	6	3	13	34	3	3	3	4(5)	0.042	0.031	36
CSE2	63	1	32	4	2	8	22	2	2	2	2(2)	0.051	0.036	41
pde	84	1	1	6	1	7	13	2	1	4	1(2)	0.158	0.034	366
CDplayer	120	2	2	2	1	5	18	1	1	1	1(1)	0.090	0.051	76
CM3	123	1	3	4	2	9	54	2	2	2	2(2)	0.208	0.133	56
heat-cont	200	1	1	2	1	2	20	1	1	1	1(1)	0.402	0.197	104
heat-disc	200	1	1	3	1	3	12	1	1	2	1(2)	0.803	0.193	317
random	200	1	1	2	1	2	11	1	1	1	1(1)	0.421	0.253	66
CM4	243	1	3	4	1	8	34	2	1	2	1(1)	1.192	0.430	178
tline	256	2	2	31	4	60	189	2	4	29	4(35)	22.486	3.148	614
iss	270	3	3	6	3	13	37	3	3	3	3(3)	2.350	1.225	92
beam	348	1	1	2	1	3	10	1	1	1	1(1)	1.284	0.872	47
CBM	351	1	2	2	1	2	11	1	1	1	1(1)	1.399	0.889	57
eady	598	1	1	2	1	5	10	1	1	1	0(0)	9.435	7.617	24
fom	1006	1	1	2	1	2	20	1	1	1	1(1)	63.508	55.808	14
Totals:				78	24	142	495	Average % faster:			139			

Table 2: The headers remain mostly as described in Table 1, except instead, in the ε -spectral value set radius, the number of circular and radial searches are given under the “circ.” and “rad.” headers, respectively.

eigenvalue-based searches.

9.2 Pseudospectral evaluation

We also evaluated our new methods against the `pspa` and `pspr` codes, using matrices of order 200 from EigTool [Wri02], with $\varepsilon = 0.01$. For brevity, we defer the full performance tables and detailed discussion to Appendix B but we note that our new method was on average 190% and 84% faster for the pseudospectral abscissa and radius cases, respectively. Only on one example, `orrsommerfeld_demo` for the abscissa case, did `pspa` incur a significant relative error (1.75×10^{-9}). Rounding errors in the eigenvalue value computations caused the horizontal searches to repeatedly overshoot the true abscissa value; `pspa` not only incurred more iterations than necessary, it did so while also making its accuracy even worse. In Figure 2, we show an example of this phenomenon when computing the pseudospectral abscissa of `orrsommerfeld_demo(201)` for $\varepsilon = 10^{-4}$, where the relative error was even more pronounced: 7.75×10^{-7} . When replacing `eig` by a structure-preserving eigensolver from SLICOT, the relative error from `pspa` was -4.68×10^{-9} .

10 Conclusion

By extending and improving upon the ε -pseudospectral abscissa and radius algorithms of [BLO03] and [MO05], we developed the first algorithms to compute, not just approximate, the general ε -spectral value set abscissa and radius to high accuracy. Our experiments validate that our new root-finding-based approach is noticeably faster and more accurate than directly-extend approaches, benefits that are also relevant for pseudospectra. The new methods also use a novel new technique for handling singular pencils and/or problematic interior searches.

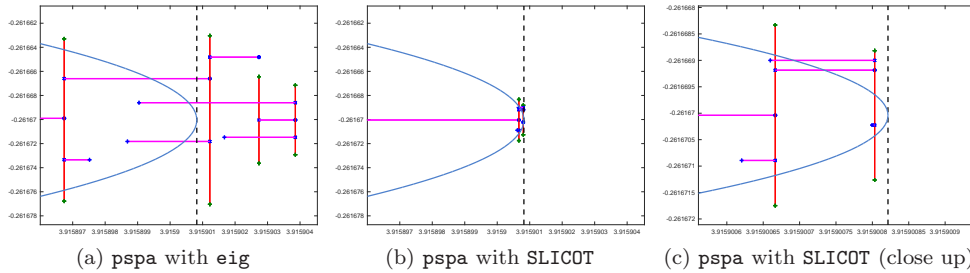


Figure 2: The plotting output of `pspa` is shown for `orrsommerfeld_demo(201)` and $\varepsilon = 10^{-4}$, demonstrating how inaccuracies in the eigensolves can lead to a significant loss of digits. The value of the pseudospectral abscissa computed by our improved method is shown by the grey dashed line, while the pseudospectral value boundary is shown by the blue curve, computed via `contour`.

Acknowledgement

The authors are grateful to the referees for many helpful comments to improve the manuscript and to Emre Mengi and Michael L. Overton for discussions regarding the numerical subtleties of their criss-cross codes for the pseudospectral abscissa and radius.

References

- [BLO03] J. V. Burke, A. S. Lewis, and M. L. Overton. Robust stability and a criss-cross algorithm for pseudospectra. *IMA J. Numer. Anal.*, 23(3):359–375, 2003.
- [BM18] P. Benner and T. Mitchell. Faster and more accurate computation of the \mathcal{H}_∞ norm via optimization. *SIAM J. Sci. Comput.*, 40(5):A3609–A3635, October 2018.
- [BMS⁺99] P. Benner, V. Mehrmann, V. Sima, S. Van Huffel, and A. Varga. SLICOT - a subroutine library in systems and control theory. In B. N. Datta, editor, *Applied and Computational Control, Signals, and Circuits*, volume 1, chapter 10, pages 499–539. Birkhäuser, Boston, MA, 1999.
- [BV14] P. Benner and M. Voigt. A structured pseudospectral method for \mathcal{H}_∞ -norm computation of large-scale descriptor systems. *Math. Control Signals Systems*, 26(2):303–338, 2014.
- [Bye88] R. Byers. A bisection method for measuring the distance of a stable to unstable matrices. *SIAM J. Sci. Statist. Comput.*, 9:875–881, 1988.
- [Dai89] L. Dai. *Singular Control Systems*. Number 118 in Lecture Notes in Control and Information Sciences. Springer-Verlag, Berlin, 1989.
- [FRM08] F. Freitas, J. Rommes, and N. Martins. Gramian-based reduction method applied to large sparse power system descriptor models. *IEEE Trans. Power Syst.*, 23(3):1258–1270, August 2008.
- [GGO13] N. Guglielmi, M. Gürbüzbalaban, and M. L. Overton. Fast approximation of the H_∞ norm via optimization over spectral value sets. *SIAM J. Matrix Anal. Appl.*, 34(2):709–737, 2013.
- [GO11] N. Guglielmi and M. L. Overton. Fast algorithms for the approximation of the pseudospectral abscissa and pseudospectral radius of a matrix. *SIAM J. Matrix Anal. Appl.*, 32(4):1166–1192, 2011.
- [HP05] D. Hinrichsen and A. J. Pritchard. *Mathematical Systems Theory I*. Springer-Verlag, Berlin, 2005.
- [HS91] D. Hinrichsen and N. K. Son. Stability radii of linear discrete-time systems and symplectic pencils. *Int. J. Robust Nonlinear Control*, 1:79–97, 1991.

- [Lan64] P. Lancaster. On eigenvalues of matrices dependent on a parameter. *Numer. Math.*, 6:377–387, 1964.
- [Lau81] A. Laub. Efficient multivariable frequency response computations. *IEEE Trans. Autom. Control*, 26(2):407–408, April 1981.
- [Men06] E. Mengi. *Measures for Robust Stability and Controllability*. PhD thesis, New York University, New York, NY 10003, USA, September 2006.
- [MO] E. Mengi and M. L. Overton. Software for Robust Stability and Controllability. <http://home.ku.edu.tr/~emengi/software/robuststability.html>.
- [MO05] E. Mengi and M. L. Overton. Algorithms for the computation of the pseudospectral radius and the numerical radius of a matrix. *IMA J. Numer. Anal.*, 25(4):648–669, 2005.
- [MO16] T. Mitchell and M. L. Overton. Hybrid expansion-contraction: a robust scaleable method for approximating the H_∞ norm. *IMA J. Numer. Anal.*, 36(3):985–1014, 2016.
- [OW95] M. L. Overton and R. S. Womersley. Second derivatives for optimizing eigenvalues of symmetric matrices. *SIAM J. Matrix Anal. Appl.*, 16(3):697–718, 1995.
- [TE05] L. N. Trefethen and M. Embree. *Spectra and pseudospectra: The behavior of nonnormal matrices and operators*. Princeton University Press, Princeton, NJ, 2005.
- [Tre99] L. N. Trefethen. Computation of pseudospectra. *Acta Numer.*, 8:247–295, 1999.
- [Van85] C. F. Van Loan. How near is a stable matrix to an unstable matrix? In *Linear algebra and its role in systems theory (Brunswick, Maine, 1984)*, volume 47 of *Contemp. Math.*, pages 465–478. Amer. Math. Soc., Providence, RI, 1985.
- [VDV85] P. Van Dooren and M. Verhaegen. On the use of unitary state-space transformations. In *Linear algebra and its role in systems theory (Brunswick, Maine, 1984)*, volume 47 of *Contemp. Math.*, pages 447–463. Amer. Math. Soc., Providence, RI, 1985.
- [Wri02] T. G. Wright. EigTool. <http://www.comlab.ox.ac.uk/pseudospectra/eigtool/>, 2002.
- [WT01] T. G. Wright and L. N. Trefethen. Large-scale computation of pseudospectra using ARPACK and eigs. *SIAM J. Sci. Comput.*, 23(2):591–605, 2001. Copper Mountain Conference (2000).

Supplementary Appendices

A Proofs of Theorems 3.1, 3.4, and 5.1

A.1 Proof of Theorem 3.1

Proof. Let γ be a singular value of $G(x+\mathbf{i}y)$ with left and right singular vectors u and v , that is, so that $G(x+\mathbf{i}y)v = \gamma u$ and $G(x+\mathbf{i}y)^*u = \gamma v$. Using the expanded versions of these two equivalences

$$\begin{aligned} \left(C((x+\mathbf{i}y)E - A)^{-1}B + D \right) v &= \gamma u \quad \text{and} \\ \left(C((x+\mathbf{i}y)E - A)^{-1}B + D \right)^* u &= \gamma v, \end{aligned} \quad (30)$$

we define

$$q = ((x+\mathbf{i}y)E - A)^{-1}Bv \quad \text{and} \quad s = ((x-\mathbf{i}y)E^* - A^*)^{-1}C^*u. \quad (31)$$

Rewriting (30) using (31) yields the following matrix equation:

$$\begin{bmatrix} C & 0 \\ 0 & B^* \end{bmatrix} \begin{bmatrix} q \\ s \end{bmatrix} = \begin{bmatrix} -D & \gamma I \\ \gamma I & -D^* \end{bmatrix} \begin{bmatrix} v \\ u \end{bmatrix} \implies \begin{bmatrix} v \\ u \end{bmatrix} = \begin{bmatrix} -D & \gamma I \\ \gamma I & -D^* \end{bmatrix}^{-1} \begin{bmatrix} C & 0 \\ 0 & B^* \end{bmatrix} \begin{bmatrix} q \\ s \end{bmatrix}, \quad (32)$$

where

$$\begin{bmatrix} -D & \gamma I \\ \gamma I & -D^* \end{bmatrix}^{-1} = \begin{bmatrix} -R^{-1}D^* & -\gamma R^{-1} \\ -\gamma S^{-1} & -DR^{-1} \end{bmatrix} \quad \text{and} \quad \begin{bmatrix} q \\ s \end{bmatrix} \neq 0. \quad (33)$$

Rewriting (31) as a matrix equation gives:

$$\left(\begin{bmatrix} (x+\mathbf{i}y)E & 0 \\ 0 & (x-\mathbf{i}y)E^* \end{bmatrix} - \begin{bmatrix} A & 0 \\ 0 & A^* \end{bmatrix} \right) \begin{bmatrix} q \\ s \end{bmatrix} = \begin{bmatrix} B & 0 \\ 0 & C^* \end{bmatrix} \begin{bmatrix} v \\ u \end{bmatrix}. \quad (34)$$

Substituting in (32) for the rightmost term of (34) yields

$$\left(\begin{bmatrix} (x+\mathbf{i}y)E & 0 \\ 0 & (x-\mathbf{i}y)E^* \end{bmatrix} - \begin{bmatrix} A & 0 \\ 0 & A^* \end{bmatrix} \right) \begin{bmatrix} q \\ s \end{bmatrix} = \begin{bmatrix} B & 0 \\ 0 & C^* \end{bmatrix} \begin{bmatrix} -D & \gamma I \\ \gamma I & -D^* \end{bmatrix}^{-1} \begin{bmatrix} C & 0 \\ 0 & B^* \end{bmatrix} \begin{bmatrix} q \\ s \end{bmatrix}. \quad (35)$$

Bringing over terms from the left side to separate out $\mathbf{i}y$ and substituting the inverse on the right using (33) and then multiplying out the matrix terms, we have

$$\mathbf{i}y \begin{bmatrix} E & 0 \\ 0 & E^* \end{bmatrix} \begin{bmatrix} q \\ s \end{bmatrix} = \begin{bmatrix} A - xE & 0 \\ 0 & A^* - xE^* \end{bmatrix} \begin{bmatrix} q \\ s \end{bmatrix} + \begin{bmatrix} -BR^{-1}D^*C & -\gamma BR^{-1}B^* \\ -\gamma C^*S^{-1}C & -C^*DR^{-1}B^* \end{bmatrix} \begin{bmatrix} q \\ s \end{bmatrix}.$$

Combining the matrices on the right and multiplying by

$$\begin{bmatrix} I & 0 \\ 0 & -I \end{bmatrix}$$

yields:

$$\mathbf{i}y \begin{bmatrix} E & 0 \\ 0 & E^* \end{bmatrix} \begin{bmatrix} q \\ s \end{bmatrix} = \begin{bmatrix} (A - xE - BR^{-1}D^*C) & -\gamma BR^{-1}B^* \\ \gamma C^*S^{-1}C & -(A - xE - BR^{-1}D^*C)^* \end{bmatrix} \begin{bmatrix} q \\ s \end{bmatrix}.$$

It is now clear that $\mathbf{i}y$ is an eigenvalue of the matrix pencil $(\mathcal{M}_{\gamma x}, \mathcal{N})$.

Now suppose that $\mathbf{i}y$ is an eigenvalue of pencil $(\mathcal{M}_{\gamma x}, \mathcal{N})$ with eigenvector given by q and s as above. Then it follows that (35) holds, which can be rewritten as (34) by defining u and v using the right-hand side equation of (32), noting that neither can be identically zero. It is then clear that the two equivalences in (31) both hold. Finally, substituting (31) into the left-hand side equation of (32), it is clear that γ is a singular value of $G(x+\mathbf{i}y)$, with left and right singular vectors u and v . \square

A.2 Proof of Theorem 3.4

Proof. By Theorem 3.1 and Corollary 2.5, $-s + \mathbf{i}\omega_j$ must be all the boundary points of $\sigma_\varepsilon(e^{\mathbf{i}\theta_r}A, e^{\mathbf{i}\theta_r}B, C, D, E)$ along the vertical line defined by $x = -s$. Recalling (3), since this spectral value set is entirely composed of eigenvalues of $(e^{\mathbf{i}\theta_r}M(\Delta), E)$, multiplying $e^{\mathbf{i}\theta_r}M(\Delta)$ by $e^{-\mathbf{i}\theta_r}$ is equivalent to a rotation about the origin by angle $-\theta_r$, which yields $\sigma_\varepsilon(A, B, C, D, E)$. Since $\theta_r = \pi/2 - \theta$, this specific rotation also moves all points $-s + \mathbf{i}\omega_j$ precisely onto the line $L(\theta, s)$ and thus $\lambda_j = e^{-\mathbf{i}\theta_r}(-s + \mathbf{i}\omega_j)$ are all the boundary points of $\sigma_\varepsilon(A, B, C, D, E)$ along $L(\theta, s)$. \square

A.3 Proof of Theorem 5.1

Proof. Let γ be a singular value of $G(re^{\mathbf{i}\theta})$ with left and right singular vectors u and v , that is, so that $G(re^{\mathbf{i}\theta})v = \gamma u$ and $G(re^{\mathbf{i}\theta})^*u = \gamma v$. Using the expanded versions of these two equivalences

$$\left(C(re^{\mathbf{i}\theta}E - A)^{-1}B + D\right)v = \gamma u \quad \text{and} \quad \left(C(re^{\mathbf{i}\theta}E - A)^{-1}B + D\right)^*u = \gamma v, \quad (36)$$

we define

$$q = (re^{\mathbf{i}\theta}E - A)^{-1}Bv \quad \text{and} \quad s = (re^{-\mathbf{i}\theta}E^* - A^*)^{-1}C^*u. \quad (37)$$

Similar to the proof of Theorem 3.1, it follows that

$$\left(\begin{bmatrix} e^{\mathbf{i}\theta}rE & 0 \\ 0 & re^{-\mathbf{i}\theta}E^* \end{bmatrix} - \begin{bmatrix} A & 0 \\ 0 & A^* \end{bmatrix}\right) \begin{bmatrix} q \\ s \end{bmatrix} = \begin{bmatrix} B & 0 \\ 0 & C^* \end{bmatrix} \begin{bmatrix} -D & \gamma I \\ \gamma I & -D^* \end{bmatrix}^{-1} \begin{bmatrix} C & 0 \\ 0 & B^* \end{bmatrix} \begin{bmatrix} q \\ s \end{bmatrix}. \quad (38)$$

Furthermore, the rightmost three terms of (38) can again be replaced by first substituting the matrix inverse with its explicit form given by (33) and then multiplying these three terms together. Then, multiplying on the left by

$$\begin{bmatrix} I & 0 \\ 0 & -e^{\mathbf{i}\theta}I \end{bmatrix}$$

and rearranging terms yields

$$e^{\mathbf{i}\theta} \begin{bmatrix} rE & 0 \\ 0 & A^* \end{bmatrix} \begin{bmatrix} q \\ s \end{bmatrix} = \begin{bmatrix} A & 0 \\ 0 & rE^* \end{bmatrix} \begin{bmatrix} q \\ s \end{bmatrix} + \begin{bmatrix} B & 0 \\ 0 & -e^{\mathbf{i}\theta}C^* \end{bmatrix} \begin{bmatrix} -R^{-1}D^*C & -\gamma R^{-1}B^* \\ -\gamma S^{-1}C & -DR^{-1}B^* \end{bmatrix} \begin{bmatrix} q \\ s \end{bmatrix}.$$

Separating and then bringing the $-e^{\mathbf{i}\theta}$ terms over to the left side, we obtain

$$e^{\mathbf{i}\theta} \begin{bmatrix} rE & 0 \\ -\gamma C^*S^{-1}C & A^* - C^*DR^{-1}B^* \end{bmatrix} \begin{bmatrix} q \\ s \end{bmatrix} = \begin{bmatrix} A - BDR^{-1}B^* & -\gamma BR^{-1}B^* \\ 0 & rE^* \end{bmatrix} \begin{bmatrix} q \\ s \end{bmatrix},$$

and thus it is clear that $e^{\mathbf{i}\theta}$ is an eigenvalue of the matrix pencil $(\mathcal{S}_{\gamma r}, \mathcal{T}_{\gamma r})$.

The reverse implication follows similarly to the reverse argument given in Appendix A.1 for the proof of Theorem 3.1. \square

B Pseudospectral evaluation (complete version)

To compare our new improved algorithms with the original criss-cross methods for computing the pseudospectral abscissa and radius, we also tested against `pspa` and `pspr`, respectively. We used 20 of the 21 examples from EigTool, all of order 200 (i.e. $n = m = p = 200$), using $\varepsilon = 0.01$; we could not include `companion_demo` as it contains `infs` and `nans` at this size. To collect the same detailed performance data as provided in §9.1, we added simple counters inside the `pspa` and `pspr` routines. Table 3 and 4 give the respective performance comparisons for the pseudospectral abscissa and radius cases.

Note that when $B = C = I_n$ and $D = 0$, by default `specValSet` does not compute the largest singular value of $G(\lambda)$ but instead equivalently computes the reciprocal of the smallest singular value of $\lambda E - A$. This is significantly more efficient than using $G(\lambda)$, which requires $(\lambda E - A)^{-1}$. Furthermore, with this smallest singular value approach, the cost of obtaining the first and second derivatives is essentially negligible.

However, during testing and development of `specValSet`, we noticed that `svd` may sometimes return extremely inaccurate results for the smaller singular values when singular vectors are also requested (which we need for the first and second derivatives). This numerical issue appears to be due to the underlying `GESDD` routine from LAPACK, which is used in MATLAB whenever singular vectors are requested (right *and* left on R2017b and earlier and right *or* left on R2018a and newer) and the minimum dimension of the matrix is at least 26. If a given matrix A is very poorly scaled, `GESDD` tends to compute all singular values below $\|A\|_2 \cdot \epsilon_{\text{mach}}$ as all being about $\|A\|_2 \cdot \epsilon_{\text{mach}}$. This means these “computed” smaller singular values may have *zero* digits of accuracy. As this can be quite problematic, `specValSet` also allows the user to optionally revert to the more expensive choice of computing the largest singular value of $G(\lambda)$, as a temporary workaround until `svd` and `GESDD` are improved. We have notified the LAPACK maintainers and MathWorks about this issue with `GESDD` and `svd`.⁵

So far, we have only observed this bad numerical behavior of `svd` occurring on one example, `companion_demo`, which is not in our test set anyway due to its extreme scaling (the norm of `companion_demo(26)` is 6.09×10^{26} and this grows as n is increased). As such, we still used the more efficient smallest singular value of $\lambda E - A$ approach for all problems in the evaluation. Furthermore, for all, we also confirmed that there were no accuracy issues with the pseudospectral abscissa and radius values computed by our new methods. Nevertheless, it is conceivable that this numerical issue with `svd` may have resulted in less accurately computed first- and second-order derivatives, which in turn, could have caused more function evaluations in the rooting finding than should have been necessary.

Returning to our performance comparison, as mentioned in §9.2, our new method was on average 190% and 84% faster for the pseudospectral abscissa and radius cases, respectively. In contrast to our spectral value set evaluation, where the DE variants were significantly less accurate than our newer methods on four of the problems, `pspa` and `pspr` returned answers which had a high numerical agreement with the accurate values computed by our improved methods on all but one problem: `orrsommerfeld_demo` for the abscissa case, where the relative error was 1.75×10^{-9} . Rounding errors in the eigenvalue value computations caused the horizontal searches to repeatedly overshoot the true abscissa value; `pspa` not only incurred more iterations than necessary, it did so while also making its accuracy even worse. In Figure 2, an example of this phenomenon is shown for computing the pseudospectral abscissa of `orrsommerfeld_demo(201)` with $\epsilon = 10^{-4}$, where the relative error was even more pronounced: 7.75×10^{-7} . When replacing `eig` by a structure-preserving eigensolver from SLICOT, the relative error from `pspa` was -4.68×10^{-9} ; in this case, `pspa` stagnated a bit too early, due to the vertical search failing to return the vertical cross section.

In Table 3, we see that our new method was faster than `pspa` on every single test problem and 190% faster on average. The largest performance gap was on `gaussseidel(200, 'C')`, where our method was 583% faster than `pspa`. The smallest performance gap was on `chebspec(201)`, where our method was 29% faster than `pspa`. Over all problems, relative to `pspa`, we see that our method only needed about a quarter of the expensive eigenvalue computations, but required slightly more than four times the number of SVDs. Nevertheless, the tradeoff was a success given the clear overall large reductions in running times.

For the pseudospectral radius comparison, shown in Table 4, we see that our new method was faster on 19 out of the 20 problems, but to a lesser degree. At best, our new method was 357% faster than `pspr` (on `kahan(200)`) and 84% faster on average. On the only problem where our new method was slower than `pspr` (`davies(201)`), the performance difference was rather

⁵For more info, see <https://github.com/Reference-LAPACK/lapack/issues/316>.

Pseudospectral Abscissa ($\varepsilon = 0.01$): pspa versus new method											
Problem	# solves				# searches				time (sec.)	% faster	
	Eig		SVD		vert.	horz.					
airy(201)	13	4	10	38	4	4	9	4(6)	1.748	0.886	97
basor(200)	9	2	0	13	4	2	5	2(2)	1.446	0.494	193
chebspec(201)	5	2	4	34	2	2	3	2(3)	0.626	0.485	29
convdiff(201)	4	1	0	23	2	1	2	1(1)	0.349	0.188	85
davies(201)	5	1	0	6	2	1	3	1(1)	0.787	0.229	243
demmel(200)	15	6	12	75	7	6	8	6(6)	1.692	1.222	39
frank(200)	3	1	0	14	2	1	1	1(1)	0.414	0.181	129
gaussseidel(200,'C')	5	1	10	5	3	1	2	1(1)	1.013	0.148	583
gaussseidel(200,'D')	5	2	0	20	3	2	2	2(3)	0.754	0.375	101
gaussseidel(200,'U')	5	2	0	20	3	2	2	2(3)	1.044	0.536	95
grcar(200)	3	1	4	11	2	1	1	1(2)	0.418	0.205	104
hatano(200)	4	1	0	5	2	1	2	1(1)	0.598	0.121	395
kahan(200)	4	1	0	8	2	1	2	1(1)	0.478	0.138	247
landau(200)	14	2	2	13	5	2	9	2(2)	1.091	0.334	227
orrsommerfeld(201)*	15	4	2	34	7	4	8	4(4)	1.900	0.820	132
random(200)	4	2	0	16	2	2	2	2(3)	0.557	0.334	67
randomtri(200)	3	1	40	10	2	1	1	1(1)	0.639	0.152	322
rifle(200)	7	1	2	8	4	1	3	1(1)	0.427	0.099	331
transient(200)	6	2	0	16	3	2	3	2(2)	1.180	0.618	91
twisted(200)	9	2	8	14	4	2	5	2(2)	1.349	0.339	298
Totals:	138	39	94	383					Average % faster:	190	

Table 3: The headers remain as described in Table 1 in the main paper, except now performance data is given for **pspa** (left columns) and our improved approach (right columns) for computing the pseudospectral abscissa on problems from EigTool, all of order 200 ($= n = m = p$).

negligible at just 4% slower. The smaller performance improvement on the radius problems appears to be due to the fact that on ten of the problems, **pspr** only needed just one circular search before convergence was met. Indeed, compared to the abscissa case, the total number of expensive eigenvalue computations incurred by **pspr** was simply much less than that by **pspa**, as was the relative reduction of them afforded by our new method.

Pseudospectral Radius ($\varepsilon = 0.01$): <code>pspr</code> versus new method											
Problem	# solves				# searches			time (sec.)	% faster		
	Eig		SVD		circ.	rad.					
airy(201)	5	2	19	28	2	2	3	2(3)	0.953	0.800	19
basor(200)	7	2	15	18	3	2	4	2(2)	1.531	0.868	76
chebspec(201)	2	1	11	14	1	1	1	1(1)	0.315	0.292	8
convdiff(201)	2	1	9	11	1	1	1	1(1)	0.289	0.225	28
davies(201)	2	1	10	13	1	1	1	1(1)	0.409	0.424	-4
demmel(200)	2	1	7	16	1	1	1	1(1)	0.275	0.234	17
frank(200)	3	1	6	19	1	1	2	1(1)	0.494	0.290	71
gaussseidel(200,'C')	2	1	2	10	1	1	1	1(1)	0.403	0.299	35
gaussseidel(200,'D')	6	1	10	17	3	1	3	1(2)	0.993	0.312	218
gaussseidel(200,'U')	4	1	11	21	2	1	2	1(3)	1.245	0.415	200
grcar(200)	10	5	34	57	5	5	5	6(6)	1.969	1.597	23
hatano(200)	2	1	6	10	1	1	1	1(1)	0.402	0.294	37
kahan(200)	7	1	19	12	3	1	4	1(2)	1.103	0.241	357
landau(200)	7	2	16	16	3	2	4	2(2)	1.419	0.547	160
orrsommerfeld(201)	2	1	11	14	1	1	1	1(1)	0.666	0.424	57
random(200)	6	4	26	48	3	4	3	6(6)	1.546	1.368	13
randomtri(200)	5	1	15	14	2	1	3	1(2)	0.891	0.252	254
riffle(200)	2	1	2	14	1	1	1	1(2)	0.292	0.227	28
transient(200)	6	2	11	21	2	2	4	2(2)	1.755	1.009	74
twisted(200)	2	1	2	17	1	1	1	1(1)	0.412	0.411	0
Totals:		84	31	242	390	Average % faster:			84		

Table 4: The headers remain mostly unchanged from Table 3, except now `pspr` (left columns) and our improved approach (right columns) for computing the pseudospectral radius for the same problems; correspondingly, the number of circular and radial searches are respectively given under the “circ.” and “rad.” headers.